Utrecht University

Master Thesis Theoretical Physics

Fermi arcs in an exactly solvable model for cuprates

Author:
Louis Verhees *(6284655)*

Supervisor:
prof. dr. ir. Henk Stoof

February 11, 2025

Utrecht University

Contents

Abstract

In the search for room-temperature superconductors, understanding the pseudogap phase in strange metals such as cuprates is of vital importance for a possible microscopic description of high-temperature superconductivity that exceeds the BCS-theory critical temperature. In this thesis we investigate strongly correlated electron models that can describe disconnected Fermi surfaces known as Fermi arcs. In contrast to the widely used Hubbard model the model we use is exactly solvable, giving an intuitive understanding of what Fermi arcs are. We go into the properties of the Hatsugai-Kohmoto model such as spin correlation and entropy. Then we look at deviations from this model that can describe Fermi arcs exactly. After we first introduce a model that more naturally arises from the Hatsugai-Kohmoto model and supports Fermi arcs we arrive at a recently discovered model that through antiferromagnetic spin coupling on different momenta in the interaction gives a description of Fermi arcs in the nodal direction which agrees which APRES experiments on cuprates. In this model, we find a connected surface that consist of Fermi arcs and Luttinger arcs that enclose multiple ground-states in momentum space.

Chapter 1

Introduction

Research in high-temperature superconductivity has led to a vivid discussion on the emergence of Fermi arcs in strange metals such as cuprates. Cuprates are copper-oxide compound materials which exhibit high-temperature superconductivity. See a schematic representation with given orbitals in Figure (1.2). First discovered in 1986 [2], for a lanthanum-barium-copper-oxide, where a critical temperature of 30K was discovered in this material. Well above the theoretical limits of BCS theory for conventional superconductors. This means that new theoretical models have to be made to explain high-Tc superconductivity. The highest yet known temperature for superconductivity in cuprates is around 133 Kelvin at ambient pressure found in a cuprate of mercury, barium and calcium [15]. Understanding these materials better may ultimately lead to a discovery of room-temperature superconductors which will be of great importance in the energy transition and therefore a sustainable future. Energy transport with near 100 percent efficiency may be to our disposal in the future, and medical imaging devices such as MRI scans could be cheaper and easier to make. On the other hand, interesting physics is yielded in search for these room-temperature superconductors, which is of fundamental importance in a very broad scope encompassing multiple areas of physics, such as low- to high energy physics crossovers. Linear in T-resistivity in the strange metal regime. But also, in the regime where we are working in this thesis, the psuedogap phase of the cuprate phase diagram, where violations of fundamental theorems in quantum mechanics such as Luttingers theorem will arise. This two folded-ness of either high societal impact on the one hand and providing a deep understanding of fundamental physics, may be one of the reasons that the field of strongly correlated electrons and especially superconductivity is one of the biggest research areas in physics.

In this thesis we investigate the properties of cuprate materials in the pseudogap regime, this is one of the phases in the intricate phase diagram of strange metals next to the antiferromagnetic (AF) state, the superconducting phase, the strange-metal phase and the Fermi liquid phase see Figure (1.1). Upon increasing doping we go from a perfect antiferromagnetic ordered state, which is insulating, to an overdoped region where we retrieve a normal Fermi liquid, where the formalism of fermionic quasiparticles can be used in accordance with normal metals. In between we find a superconducting state where fermions form bonds and electrical resistivity goes to zero is. How this works microscopically is still unclear and needs more research. However, most interest lies not in the superconducting part of the phase diagram, but in the strange-metal phase and pseudogap phase. Because in these phases we have a departure from Fermi-liquid theory and questions about the origin of high-Tc superconductivity may be answered in these regimes.

The pseudogap region is located in the under-doped region next to non-Fermi liquid phase or strange metal phase, AF phase and superconducting phase. This phase is characterized by gaps in the Fermi surface which can be measured by APRES (angle resolved photoemission spectroscopy) experiments [13] [10]. APRES is an experimental technique used to probe the electronic structure of materials. At its core, ARPES relies on the photoelectric effect: photons strike a material, ejecting electrons whose energy and momentum carry direct information about the material's electronic states. In the pseudogap regime, a suppression of the electronic density of states is seen near the Fermi level with these experiments on cuprates.

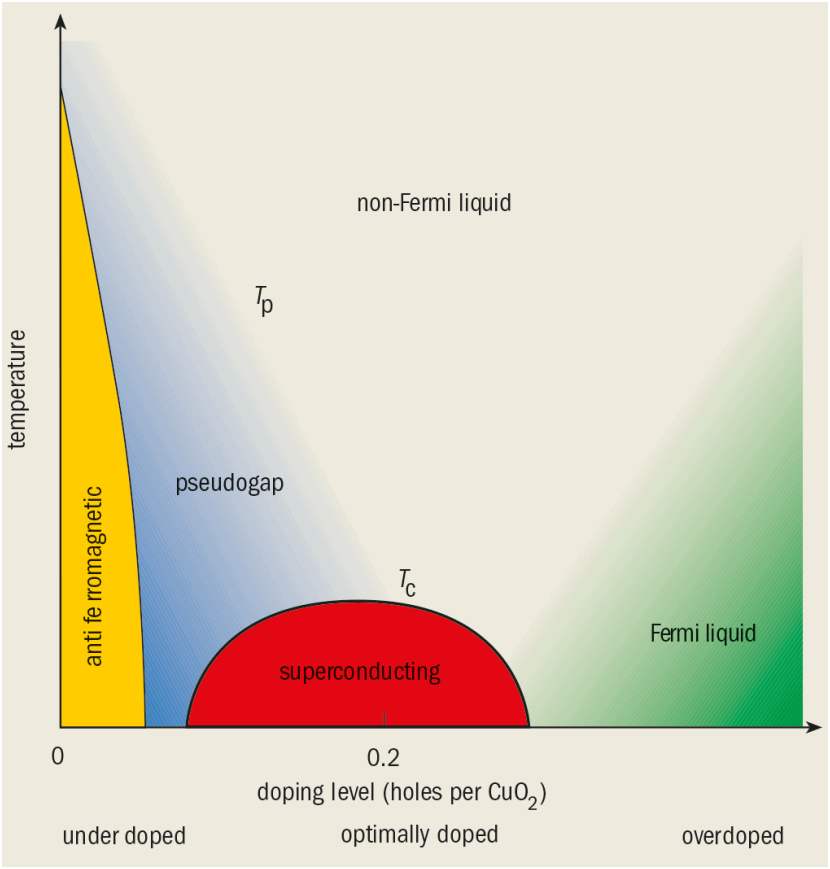

Figure 1.1: Phase diagram of strange metals. Different properties of cuprates are indicated. Cuprates are known to have one of the highest critical temperatures T_c here indicated by the thick black line. The phase diagram is gives for various temperatures and doping, where, doping refers to the creations of holes or the removing of electrons out of the CuO_2 layers in the material. [1]

The nature of this partly suppression of the Fermi surface is important to understand because it happens above the superconducting critical temperature and it can be seen a precursor of the superconducting regime, because mechanisms that govern the oppression of electronic density at certain points (Fermi arcs) may lie at the origin of mechanisms that also underlie superconductivity. For example, direct evidence of preformed Cooper pairing has been observed by Bogoliubov-like dispersion in the pseudogap phase [16].

In this thesis we will try to shed light on the origin of these pseudogaps, by looking at exactly solvable models that display Fermi arcs. We can show this by hand, without numerical calculations by introducing a new kind of interaction which differs from the more widely used Hubbard model interaction which is not exactly solvable in arbitrary dimensions in momentum space. This way we hope to give a more intuitive and intelligible picture of what happens in the pseudogap regime of cuprates.

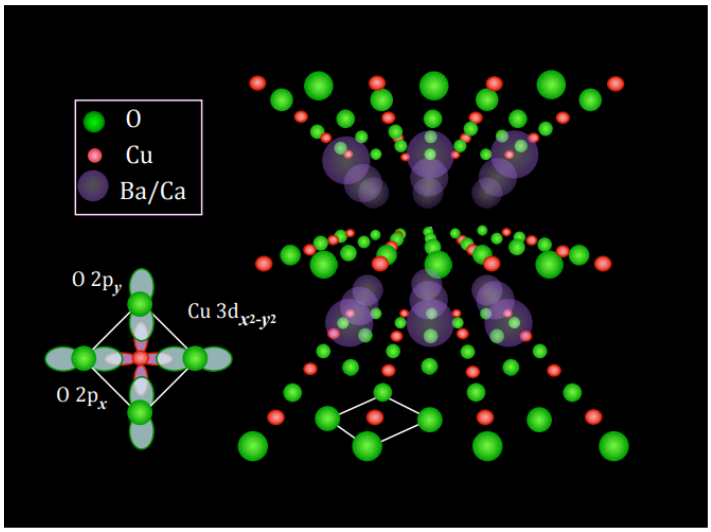

Figure 1.2: Crystal structure of a typical cuprate as described in this thesis. The $Cu0_2$ layers are separated by insulating layers of Ba/Ca.[8]

Chapter 2

Hatsugai-Kohmoto Model

The study of strongly correlated electrons relies on models that can capture the interaction between electrons, going beyond standard band theory for electrons in a lattice. A first motivation for doing this stems from the observation that certain materials exhibit a so called Mott transition. These are metals that are conducting electricity according to conventional band theory but turn out to be insulators because of electron-electron Coulomb interactions [11]. Now, a fairly simple model that includes this interaction is the famous Hubbard model[7]. This model is widely used in the study of strongly correlated electrons and gives good results when it is applied to high-temperature superconductors such as cuprates. In second quantization we can write the Hubbard Hamiltonian as

$$\hat{H}_{hubbard} = -\sum_{ij,\sigma} t_{ij}\hat{c}_{i,\sigma}\hat{c}^{\dagger}_{j,\sigma} - \mu\sum_{i}\hat{n}_i + U\sum_{i}\hat{n}_{i,\uparrow}\hat{n}_{i,\downarrow}. \tag{2.1}$$

Here, $\hat{c}^{\dagger}$ and $\hat{c}$ are the fermionic creation and annihilation operators. They satisfy the standard fermionic anti-commutaion rule $\{\hat{c}_{i\sigma}, \hat{c}^{\dagger}_{j\sigma}\} = \delta_{ij}\delta_{\sigma\sigma'}$. In addition, t_{ij} is the hopping parameter for an electron to hop from a site i to a neighboring site j in a lattice. The first term sums over the spin $\sigma = \uparrow, \downarrow$ of the electron, μ is the chemical potential which we require because we work in a grand-canonical ensemble and $\hat{n}_i$ is the number operator at a site i counting the number of electrons at a particular site. The last term represents the positive repulsive interaction which is in competition with the hopping term and therefore this model can give rise to a band gap between two energy bands, creating a Mott phase when the fermi level lies in between these bands. The interaction only works if there are two electrons at one site i, one having spin up and the other having spin down. Always having opposite spins due to Pauli exclusion principle.

Despite it being a seemingly simple model, solving it in more than one dimensions has not been achieved yet. This remains one of the largest questions in condensed-matter physics. Only approximations can be made with numerical methods to use the model in more than one dimension which is normally needed to consider experiments on real materials in nature. The model we are going to discuss in this section is very similar to the Hubbard model and also exhibits the Mottness, i.e., an insulating phase due to electron interactions. In contrast to the Hubbard model this model is exactly solvable in arbitrary dimensions. It was first introduced in 1992 by Yasuhiro Hatsugai and Mahito Kohmoto and it differs from the Hubbard model in the interaction term. They imposed a new interaction term which is *localized* in momentum space. It contains a local in $\mathbf{k}$ interaction which yields that the Hamiltonian is exactly solvable. As we shall see later the hopping term and chemical potential term are diagonal (local) in momentum space too. A consequence of this implied simplification of the Hubbard model is that, in coördinate space, this Hamiltonian has a non-local interaction.

Let's begin with the Hamiltonian of the Hatsugai-Kohmoto (HK) model in coördinate space [5]

$$\hat{H}_{HK} = -\sum_{i,j,\sigma} t_{ij}\hat{c}^{\dagger}_{i\sigma}\hat{c}_{j\sigma} - \mu\sum_{j\sigma}\hat{c}^{\dagger}_{j\sigma}\hat{c}_{j\sigma} + \frac{\mathcal{V}}{L^d}\sum_{j_1,j_2,j_3,j_4}\delta_{j_1+j_3=j_2+j_4}\hat{c}^{\dagger}_{j_1\uparrow}\hat{c}_{j_2\uparrow}\hat{c}^{\dagger}_{j_3\downarrow}\hat{c}_{j_4\downarrow}. \tag{2.2}$$

The first two terms are exactly the same as in the Hubbard model, but it differs by it's interaction. L^d is the number of sites for dimension d. The peculiarity of this interaction term lies in it's non-locality. In the next section we delve deeper into what this means for our model and how it becomes local in

momentum space. After that we will fill up the ground-state of this system which is easily done because it is local in momentum space, i.e., has a Hamiltonian diagonal in $\mathbf{k}$. After that we can calculate the Green's function of the model and investigate it's properties. Also possible problematic aspect of this model which include an non-zero entropy in the ground-state will be explored in this chapter.

2.1 Interaction

Because the HK model is based upon the Hubbard model and differs in the interaction we write out the full Hubbard interaction term

$$\hat{H}_{hubbard-interaction} = U \sum_i \hat{c}^\dagger_{i\uparrow} \hat{c}_{i\uparrow} \hat{c}^\dagger_{i\downarrow} \hat{c}_{i\downarrow}, \tag{2.3}$$

we have an interaction parameter U that works only on one site i. This is a repulsive electron-electron interaction due to the on-site Coulomb potential. It is reasonable to assume because the Coulomb potential is minimized when a pair of electrons is far apart so only when they are localized on one site they 'feel' a repulsive interaction. This makes it purely local in coördinate space which is, quite straight-forward and physically an accurate description of what would happen on this scale because it captures basic electrostatics. Despite this simple local interaction the Hubbbard model cannot be solved in higher dimensions than one, because of the non-local hopping term in the coördinate space, going to the momentum space will get the first two terms in the Hubbard Hamiltonian local in $\mathbf{k}$ but not the interaction term. Now the questions may arise: Can we modify the interaction in the Hubbard model such that it also becomes local in $\mathbf{k}$-space? This is what's done in the Hastugai-Kohmoto model.

Let's look at the HK interaction in coördinate space

$$\hat{H}_{interaction} = \frac{\mathcal{V}}{L^d} \sum_{j_1,j_2,j_3,j_4} \delta_{j_1+j_3=j_2+j_4} \hat{c}^\dagger_{j_1\uparrow} \hat{c}_{j_2\uparrow} \hat{c}^\dagger_{j_3\downarrow} \hat{c}_{j_4\downarrow}, \tag{2.4}$$

where we see a summation over j_1, j_2, j_3, j_4 which are independent lattice sites. That means the interaction can be between any of the sites on the lattice giving an non-local all-to-all interaction in coörirdinate (position) space. In contrast, the Hubbard interaction is local in position space because we sum over one site i for each c-electron operator $\hat{c}^{(\dagger)}_{i,\sigma}$. Summing over $j_1 ... j_4$ independently for all creation and annihilation operators in the HK interaction highlights the nature of the non-locality of this interaction.

The Kronecker delta term in the interaction term ensures that the interaction is only non-zero if the electrons scatter in such a way that their position vectors satisfy the constraint of center-of-mass conservation (i.e. conservation of total momentum). This is illustrated in Figure (2.1). It is because of this constraint that after we do a Fourier transform we get an interaction term in the Hamiltonian that is localized in momentum space. So the interaction is non-local in real space but local in momentum space after Fourier transform.

We write a discrete Fourier transform of the creation/annihilation operators,

$$\hat{c}_{j\sigma} = \frac{1}{L^{d/2}} \sum_k e^{ik\cdot r_j} \hat{c}_{k\sigma} \tag{2.5}$$

$$\hat{c}^\dagger_{j\sigma} = \frac{1}{L^{d/2}} \sum_k e^{-ik\cdot r_j} \hat{c}^\dagger_{k\sigma} \tag{2.6}$$

where the factor $L^{d/2}$ ensures that we still retrieve the usual commutation relation $[\hat{c}^\dagger_{j\sigma}, \hat{c}_{i\sigma}] = \delta_{j,i}$ and r_j is a position vector of the electron when going to momentum space. Substituting these in the Hamiltonian we get (see appendix A)

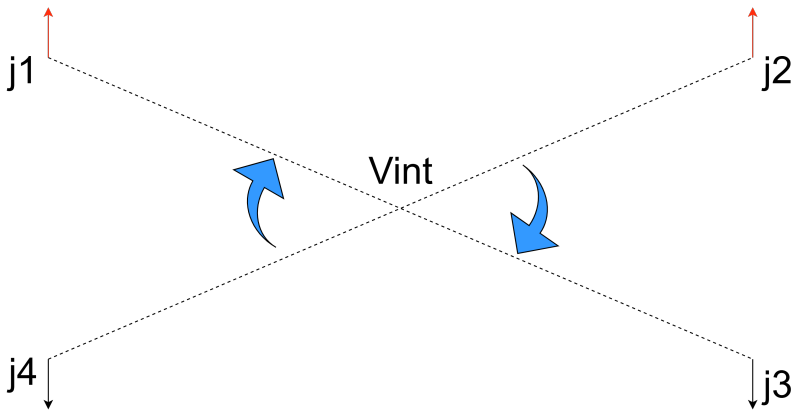

Figure 2.1: Schematic representation of the interaction as scattering. Dashed lines indicate the interaction between up and down spin electrons located at lattice points j_1, j_3 and j_2, j_4. distance of sites $r_{j_1} + r_{j_3}$ for outgoing creation operators should equal $r_{j_2} + r_{j_4}$ for annihilation operators, to ensure conservation of momenta given by the constraint $\delta_{j_1+j_3=j_2+j_4}$. The blue arrows here indicate that we annihilate on sites j_2, j_4 and create on sites j_1, j_3 follwing from $\hat{c}^\dagger_{j_1\uparrow}\hat{c}_{j_2\uparrow}\hat{c}^\dagger_{j_3\downarrow}\hat{c}_{j_4\downarrow}$.

$$\hat{H}_{interaction} = \frac{\mathcal{V}}{L^d}\sum_{j_1..j_4}\delta_{j_1+j_3=j_2+j_4}\frac{1}{L^{2d}}\sum_{k_1..k_4} e^{-ik_1\cdot r_1}\hat{c}^\dagger_{k_1\uparrow}e^{ik_2\cdot r_2}\hat{c}_{k_2\uparrow}e^{-ik_3\cdot r_3}\hat{c}^\dagger_{k_3\downarrow}e^{ik_4\cdot r_4}\hat{c}_{k_4\downarrow} \tag{2.7}$$

$$= \mathcal{V}\sum_k \hat{c}^\dagger_{k\uparrow}\hat{c}_{k\uparrow}\hat{c}^\dagger_{k\downarrow}\hat{c}_{k\downarrow} \tag{2.8}$$

and we conclude that the interaction is localized in momentum space, for every k there is only one interaction term i.e. each k state contributes independently to the partition function making the Hamiltonian diagonal and exactly solvable. This is done in next section, where we also derive the Green's function.

2.2 Exact Hamiltonian and Green's function

Having the Fourier transform of the interaction term of the HK Hamiltonian we can also do that for the hopping term and chemical potential term such that the Hamiltonian becomes perfectly diagonal in k space. After that we can fill the ground-state of the system to get the ground-sate energies. Using the Lehmann representation of the Green's function we can give an exact Green's function of this system from which we can extract insightful information such as a phase-diagram.

For completeness, we give the Fourier transform of the hopping term. From equation 2.2 we start with:

$$\hat{H}_{hopping} = -\sum_{ij,\sigma}\hat{c}_{i,\sigma}t_{ij}\hat{c}^\dagger_{j,\sigma}, \tag{2.9}$$

where i and j are neighboring sites. For simplicity we want to consider a 1 dimensional lattice, but

this is easily generalizable to 2d and 3d lattices. In 1d we get

$$\hat{H}_{hopping} = -t \sum_{j,\sigma} \left[\hat{c}^\dagger_{j+1,\sigma} \hat{c}_{j,\sigma} + \hat{c}^\dagger_{j-1,\sigma} \hat{c}_{j,\sigma} \right], \tag{2.10}$$

$$= -t \sum_{j,\sigma} \left[\hat{c}^\dagger_{j+1,\sigma} \hat{c}_{j,\sigma} + \hat{c}^\dagger_{j,\sigma} \hat{c}_{j+1,\sigma} \right], \tag{2.11}$$

$$= -t \sum_{j,\sigma} \frac{1}{L^{1/2}} \frac{1}{L^{1/2}} \sum_{k_1} \sum_{k_2} \left[e^{-ik_1(j+1)} e^{ik_2 j} + e^{-ik_1 j} e^{ik_2(j+1)} \right] \hat{c}^\dagger_{k_1\sigma} \hat{c}_{k_2,\sigma}, \tag{2.12}$$

$$= -t \frac{1}{L} \sum_{k_1,k_2} \sum_{\sigma} \sum_{j} e^{-i(k_1-k_2)j} \left[e^{-ik_1} + e^{ik_2} \right] \hat{c}^\dagger_{k_1\sigma} \hat{c}_{k_2,\sigma}, \tag{2.13}$$

$$= -t \frac{1}{L} \sum_{k_1,k_2} \sum_{\sigma} \delta_{k_1,k_2} L \left[e^{-ik_1} + e^{ik_2} \right] \hat{c}^\dagger_{k_1\sigma} \hat{c}_{k_2,\sigma}, \tag{2.14}$$

$$= -t \sum_{\mathbf{k}} \sum_{\sigma} \left[e^{-i\mathbf{k}} + e^{i\mathbf{k}} \right] \hat{c}^\dagger_{\mathbf{k}\sigma} \hat{c}_{\mathbf{k},\sigma}, \tag{2.15}$$

$$= \sum_{k,\sigma} \epsilon_k \hat{n}_{k\sigma}, \tag{2.16}$$

Where $\epsilon_k = -2t\cos(k)$ for dimension 1 or $\epsilon_k = -2t\sum_{n=1}^{d}\cos(k_n)$ for dimension d. In later models we will use a dispersion which includes hopping parameters t' and t'' for next(to next)-nearest neighbors when we also want to compare with experimental findings. For now we are going to use this dispersion relation in the rest of this chapter because it capture the relevant physics. Including also the chemical potential which is trivially also local in momentum space $\mu \sum_{j,\sigma} \hat{c}^\dagger_{j\sigma} \hat{c}_{j\sigma} = \mu \sum_{\mathbf{k},\sigma} e^{i\mathbf{k}(1-1)j} \hat{c}^\dagger_{\mathbf{k}\sigma} \hat{c}_{\mathbf{k}\sigma} = \mu \sum_{\mathbf{k},\sigma} \hat{n}_{\mathbf{k},\sigma}$.

The Hamiltonian is now fully localized in k space. This means we can write the Hamiltonian as

$$\hat{H} = \sum_{\mathbf{k}} H_{\mathbf{k}}, \tag{2.17}$$

with

$$H_{\mathbf{k}} = \sum_{\sigma} \left[(\epsilon_{\mathbf{k}} - \mu) \hat{n}_{\mathbf{k}\sigma} + \frac{\mathcal{V}}{2} \hat{n}_{\mathbf{k}\sigma} \hat{n}_{\mathbf{k}-\sigma} \right], \tag{2.18}$$

or

$$\hat{H}_{\mathbf{k}} = \sum_{\sigma} (\epsilon_{\mathbf{k}} - \mu) \hat{n}_{\mathbf{k}\sigma} + \mathcal{V} \hat{n}_{\mathbf{k}\uparrow} \hat{n}_{\mathbf{k}\downarrow}. \tag{2.19}$$

Because, an $|\uparrow\downarrow\rangle$ state is indistinguishable from a $|\downarrow\uparrow\rangle$ state.

For calculating the ground-state energies of our system we remark that the eigenstates are tensor product of the every momentum state, such that

$$|\Psi\rangle = \otimes_k |\phi_k\rangle, \tag{2.20}$$

which lives in a Fock space of k-independent Hilbert spaces. i.e.

$$\mathcal{F} = \otimes_k \mathcal{H}_k. \tag{2.21}$$

Filling up the ground-states of this system we first need to take into account that we are considering fermions which, by the Pauli exclusion principle, can never take up the same state (having all their quantum numbers the same). In our model an electron can have spin up or down. That means we have four possibilities: $|\phi_k\rangle = |0\rangle$ the vacuum state with zero particles, $|\phi_k\rangle = \hat{c}^\dagger_{k,\uparrow}|0\rangle$ or $|\phi_k\rangle = \hat{c}^\dagger_{k,\downarrow}|0\rangle$ for a singly-occupied state, and $|\phi_k\rangle = \hat{c}^\dagger_{k,\uparrow}\hat{c}^\dagger_{k,\downarrow}|0\rangle$ giving a doubly-occupied state. Filling the ground-state than gives

$$|\Psi_G\rangle_\sigma = \prod_{k\in\Omega_1} \hat{c}^\dagger_{k,\sigma} \prod_{k\in\Omega_2} \hat{c}^\dagger_{k,\sigma}\hat{c}^\dagger_{k,-\sigma}\,|0\rangle\,, \tag{2.22}$$

where Ω_1 is the region in momentum space where we have single occupation and Ω_2 is the region where we have double occupation when $k \leq k_F$. For an repulsive interaction it means that it depends on k and the Fermi momentum k_F which ground-state energy we get. (for a attractive interaction it would all be doubly occupied and $|\Psi_G\rangle = \prod_{k\leq k_F} \hat{c}^\dagger_{k,\uparrow}\hat{c}^\dagger_{k,\downarrow}\,|0\rangle$). Where the Fermi energy lies and so which ground-state configuration we have depends on our choice for the parameters of the chemical potential μ and interaction $\mathcal{V}$ which will become more clear when we will set up the phase diagram later in this chapter. For now, we need to know what the energy is for every different ground-state. They are given by

- $\hat{H}_\mathbf{k}\,|0\rangle = 0\,|0\rangle$ for the zero occupied state
- $\hat{H}_\mathbf{k}\hat{c}^\dagger_{k,\sigma}\,|0\rangle = \hat{H}_\mathbf{k}\,|1\rangle = (\epsilon_k - \mu)\,|1\rangle = \xi_k\,|1\rangle$ for the singly occupied state being either $|\uparrow\rangle$ or $|\downarrow\rangle$
- $\hat{H}_\mathbf{k}\hat{c}^\dagger_{k,\sigma}\hat{c}^\dagger_{k,-\sigma}\,|0\rangle = \hat{H}_\mathbf{k}\,|2\rangle = (2(\epsilon_k - \mu) + \mathcal{V}) = (2\xi_k + \mathcal{V})\,|2\rangle$ for doubly occupied state $|\uparrow\downarrow\rangle = |\downarrow\uparrow\rangle$,

where we used short hand notation $\xi_k = \epsilon_k - \mu$. Now with these exact ground-states and ground-state energies we can calculate the exact Green's function.

We use the definition of the retarded Green's function for fermions

$$G^R_{\mathbf{k}\sigma}(t-t') = -i\theta(t-t')\langle[\hat{c}_{\mathbf{k}\sigma}(t), \hat{c}^\dagger_{\mathbf{k}\sigma}(t')]_+\rangle \tag{2.23}$$

$$= -i\theta(t-t')[\langle\hat{c}_{\mathbf{k}\sigma}(t)\hat{c}^\dagger(t')_{\mathbf{k}\sigma}\rangle + \langle\hat{c}^\dagger_{\mathbf{k}\sigma}(t')\hat{c}_{\mathbf{k}\sigma}(t)\rangle]. \tag{2.24}$$

Here, $\hat{c}^\dagger$ and $\hat{c}$ are the creation and annihilation operators, respectively, for electrons, and $\theta(t)$ is the Heaviside step function. If we use the definition of the average value

$$\langle\hat{c}_{\mathbf{k}\sigma}(t)\hat{c}^\dagger_{\mathbf{k}\sigma}(t')\rangle = \frac{1}{Z}\sum_n e^{-\beta E_n}\,\langle n|\hat{c}_{\mathbf{k}\sigma}(t)\hat{c}^\dagger_{\mathbf{k}\sigma}(t')|n\rangle \tag{2.25}$$

$$= \frac{1}{Z}\sum_n e^{-\beta E_n}\,\langle n|e^{iHt}\hat{c}_{\mathbf{k}\sigma}(0)e^{-iHt}e^{iHt'}\hat{c}^\dagger_{\mathbf{k}\sigma}(0)e^{-iHt'}|n\rangle\,. \tag{2.26}$$

In the last line, we have written out the time dependence of the creation/annihilation operators through the Heisenberg relation. Adding a closure relation $1 = \sum_m |m\rangle\,\langle m|$, we get

$$\langle\hat{c}_{\mathbf{k}\sigma}(t)\hat{c}^\dagger_{\mathbf{k}\sigma}(t')\rangle = \frac{1}{Z}\sum_{n,m} e^{-\beta E_n}\,\langle n|e^{iHt}\hat{c}_{\mathbf{k}\sigma}e^{-iHt}\,|m\rangle\,\langle m|\,e^{iHt'}\hat{c}^\dagger_{\mathbf{k}\sigma}e^{-iHt'}|n\rangle \tag{2.27}$$

$$= \frac{1}{Z}\sum_{n,m} e^{-\beta E_n}e^{i(t-t')(E_n-E_m)}\,\langle n|\hat{c}_{\mathbf{k}\sigma}|m\rangle\,\langle m|\hat{c}^\dagger_{\mathbf{k}\sigma}|n\rangle \tag{2.28}$$

$$\tag{2.29}$$

and for the second term in equation(2.24),

$$\langle\hat{c}^\dagger_{\mathbf{k}\sigma}(t')\hat{c}_{\mathbf{k}\sigma}(t)\rangle = \frac{1}{Z}\sum_{n,m} e^{-\beta E_n}\,\langle n|e^{iHt'}\hat{c}^\dagger_{\mathbf{k}\sigma}e^{-iHt'}\,|m\rangle\,\langle m|\,e^{iHt}\hat{c}_{\mathbf{k}\sigma}e^{-iHt}|n\rangle \tag{2.30}$$

$$= \frac{1}{Z}\sum_{n,m} e^{-\beta E_n}e^{i(t-t')(E_m-E_n)}\,\langle n|\hat{c}^\dagger_{\mathbf{k}\sigma}|m\rangle\,\langle m|\hat{c}_{\mathbf{k}\sigma}|n\rangle \tag{2.31}$$

$$= \frac{1}{Z}\sum_{m,n} e^{-\beta E_m}e^{i(t-t')(E_n-E_m)}\,\langle n|\hat{c}_{\mathbf{k}\sigma}|m\rangle\,\langle m|\hat{c}^\dagger_{\mathbf{k}\sigma}|n\rangle\,, \tag{2.32}$$

where in the last line we switched summation indices m and n. Given these terms, equation (2.24) gives us the retarded Green's function

$$G^R_{k\sigma}(t) = -i\theta(t)\frac{1}{Z}\sum_{n,m}(e^{-\beta E_n} + e^{-\beta E_m})e^{it(E_n - E_m)} \langle n|\hat{c}_{\mathbf{k}\sigma}|m\rangle \langle m|\hat{c}^\dagger_{\mathbf{k}\sigma}|n\rangle , \tag{2.33}$$

where we assumed $t' = 0$.

Summing over all possible eigenstates with corresponding eigenvalues we get in our case

$$G^R_{k\sigma}(t) = -i\theta(t)\left[\frac{1 + e^{-\beta\xi_\mathbf{k}}}{Z}e^{-it\xi_\mathbf{k}} \langle 0|0\rangle \langle 1|1\rangle + \frac{e^{-\beta\xi_\mathbf{k}} + e^{-\beta(2\xi_\mathbf{k}+\mathcal{V})}}{Z}e^{-it(\xi_\mathbf{k}+\mathcal{V})} \langle 1|1\rangle \langle 2|2\rangle\right], \tag{2.34}$$

with,

$$\langle \hat{n}_{\mathbf{k}\sigma}\rangle = \frac{e^{-\beta\xi_\mathbf{k}} + e^{-\beta(2\xi_\mathbf{k}+\mathcal{V})}}{Z} \tag{2.35}$$

we get

$$G^R_{\mathbf{k}\sigma}(t) = -i\theta(t)\left[(1 - \langle \hat{n}_{\mathbf{k}\sigma}\rangle)e^{-it\xi_\mathbf{k}} + \langle \hat{n}_{\mathbf{k}\sigma}\rangle e^{-it(\xi_\mathbf{k}+\mathcal{V})}\right], \tag{2.36}$$

and when Fourier transformed this gives

$$G^R_{\mathbf{k}\sigma}(\omega) = \frac{\langle \hat{n}_{\mathbf{k}\sigma}\rangle}{\omega + \mu - \epsilon_\mathbf{k} + i0^+} + \frac{1 - \langle \hat{n}_{\mathbf{k}\sigma}\rangle}{\omega + \mu - \epsilon_\mathbf{k} - \mathcal{V} + i0^+}. \tag{2.37}$$

Note that this is the retarded green's function because we use the analytical continuation $i\omega \to \omega + i0^+$, which we can do because equation (2.37) is purely analytical in the upper half plane.

Depending on the average value of the number operator $\langle \hat{n}_{\mathbf{k}\sigma}\rangle$ we have three possibilities for our Green's function. First, a non-interacting Green's function if $\langle \hat{n}_{\mathbf{k}\sigma}\rangle = 0$. This is the first term in equation (2.37). Second, a non-interacting Green's function but with a chemical potential shifted by $\mathcal{V}$ given by the second term in equation (2.37) when $\langle \hat{n}_{\mathbf{k}\sigma}\rangle = 1$. Now with $0 < \langle \hat{n}_{\mathbf{k}\sigma}\rangle < 1$ both terms of the Green's function are non-zero and the spectral function will split into two peaks, given by two bands. The spectrum now consist of a 'lower band ' and 'upper band' that, when the interaction potential $\mathcal{V}$ is high enough, will give rise to gap in between, see Figure (2.2). When the Fermi level ($\omega = 0$) lies in between the two bands and we are in the ground-state, the lower band is completely filled such that it has no free electrons available. Energy levels of the electrons are filled up to the Fermi energy, so if the upper band is higher than the Fermi level no electrons can move in that band freely neither, resulting in an insulating phase, i.e., the Mott insulating phase. Like the Hubbard model the HK model serves as a prototypical model for a Mott insulator above a critical interaction strength $\mathcal{V}$. But, in contrast to the Hubbard model now with an exact Green's function in arbitrary dimensions in momentum space.

2.3 Zeros and occupation of the ground-state

Given that the Green's function in equation (2.45) consist of two terms, a possibility arises for them to cancel each other out such that the Green's function becomes zero under certain conditions. This has profound consequences and is of great importance for the explanation of so called Fermi arcs later in this thesis. It happens when both terms are active so for $0 < \hat{n}_{\mathbf{k}\sigma} < 1$, so there is no full occupation of every possible state and no zero occupation. Given we only have three possible configurations, namely zero $|0\rangle$, $|\uparrow\rangle$ / $|\downarrow\rangle$ or double occupation $|\uparrow\downarrow\rangle$ for fermions, we conclude that the zero points of the Green's function or zeros correspond to an occupation of $\hat{n}_{\mathbf{k}\sigma} = 1/2$, i.e., half filling or single occupation. Resolving equation (2.45) for $G^R_{\mathbf{k}\sigma}(\omega) = 0$ at this condition we see that it becomes zero at $\omega = \epsilon_k - \mu + \frac{1}{2}\mathcal{V}$. Next to peaks of the spectral function (poles) we also have zeros which can be plotted next to the poles of the Green's function. In a Mott insulating phase where the Green's functions is splitted around the Fermi level this corresponds to full band of zeros see Figure (2.3). Here the occupation is the the same for all momentum k. If we lower the chemical potential μ and interaction $\mathcal{V}$ the occupation number varies over k because the lower band moves above the Fermi level ($\omega = 0$) resulting in zero occupation (empty band), and the upper band can move below the Fermi level resulting in double occupation. Here the Green's function collapses to one term with spectral

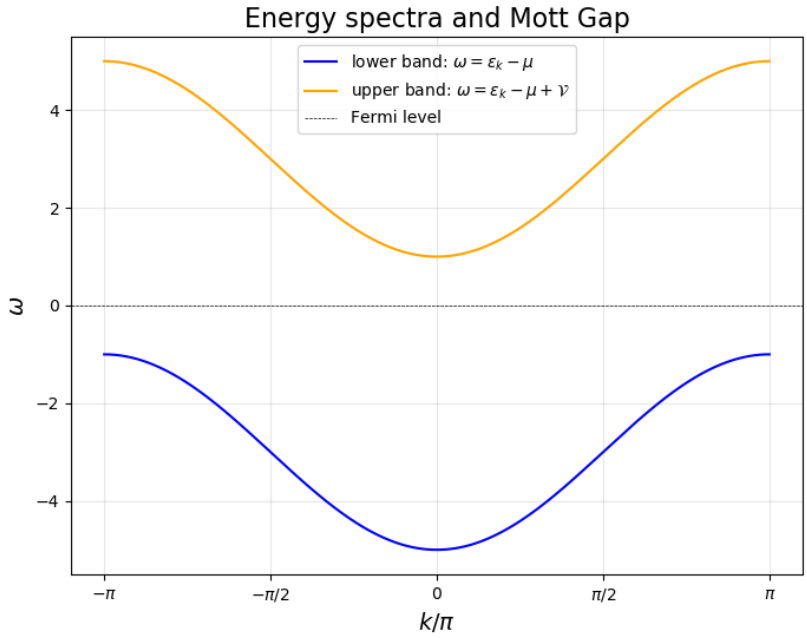

Figure 2.2: Fermi level lies in a gap between two energy bands of the Green's function for a simple 1D dispersion $\epsilon_k = -2t\cos(k)$. This indicates the Mott insulating phase

.

weight of 1 given by either the first term in equation(2.45) for zero occupation, i.e., $\hat{n}_{\mathbf{k}\sigma} = 0$ or only the second term when $\hat{n}_{\mathbf{k}\sigma} = 1$ i.e. full occupation with two electrons per k, see Figure (2.4)

The occupation regions given by Figure (2.4) also follow directly from the ground-state energies given in equation (2.31). Given that the ground-state corresponds to the lowest possible eigenenergy of the system

- Ω_0: is given by $0 < \xi_k < 2\xi_k + \mathcal{V}$, i.e., lowest energy is the vacuum state $|0\rangle$ with zero energy.
- Ω_1: is given by $\xi_k < 0$ and $\xi_k < 2\xi_k + \mathcal{V} \rightarrow \xi_k + \mathcal{V} > 0$
- Ω_2: is given by $2\xi_k + \mathcal{V} < \xi_k \rightarrow \xi_k + \mathcal{V} < 0$.

As can be seen in Figure (2.4)

2.4 Spin, magnetization and entropy

Any strongly correlated electron model such as the HK model should include an analysis for spin correlations. As can already been seen from the Hamiltonian our system has no term including any spin alignment across the lattice. If the interaction potential is a repulsive one as is the case in our model $\mathcal{V} > 0$ it will cost the electrons energy to form double-occupied k states, resulting in a single-occupied state as seen in Fig.(2.4). Aligning of the electron spins in an anti-ferromagnetic order will cost the system energy given that $\mathcal{V}$ is high enough. Therefore the system lacks any form of spin alignment in the single-occupied state region Ω_1.

A significant consequence of this, is that the ground-state for the singly occupied regions Ω_1 is highly degenerated. Every electron could have either spin up or spin down with no favorable alignment. Given that both the two spin states are equally likely and we have N lattice sites the ground-state has 2^N configurations see Fig.(2.5). This results in a non-zero entropy at T=0.

For Ω_2 we have double occupation with spin up and spin down electrons occupying the same k state, $|\uparrow\downarrow\rangle$ and $|\downarrow\uparrow\rangle$ are indistinguishable so no magnetic order can be derived in this region of momentum

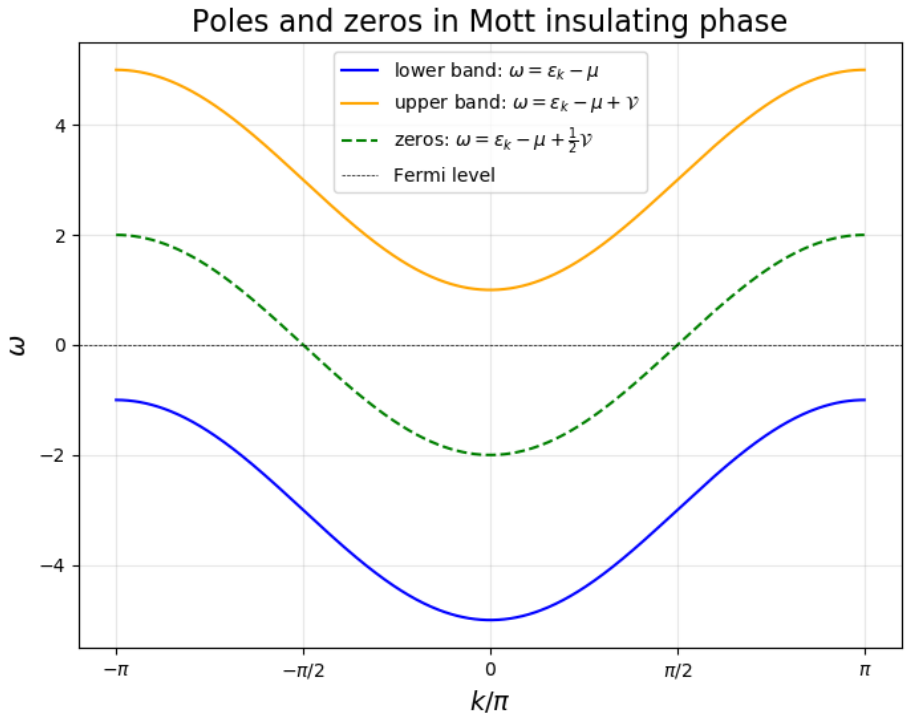

Figure 2.3: Poles and zeros of the Green's function equation (2.45). Upper and lower band are poles the Green's function both with weight 1/2. Green line represents the zeros of the Green's function

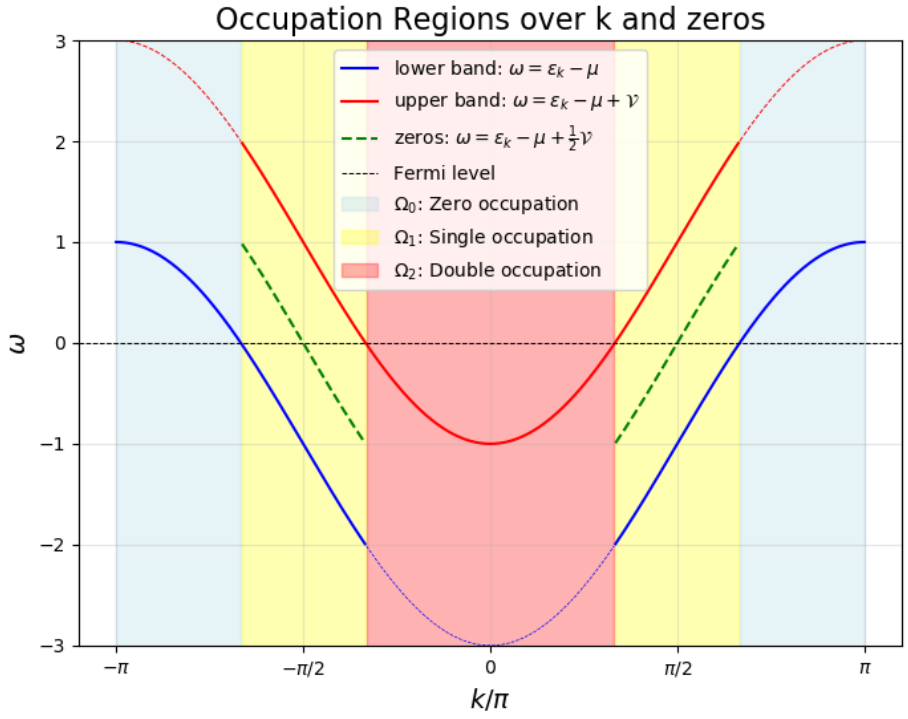

Figure 2.4: Different regions of occupation for a simple 1D dispersion, given a ground-state configuration. States are occupied up to the Fermi level of $\omega = 0$. Dashed blue and red lines indicate those momenta for which these bands are not active, i.e., the Green's function collapses to one term.

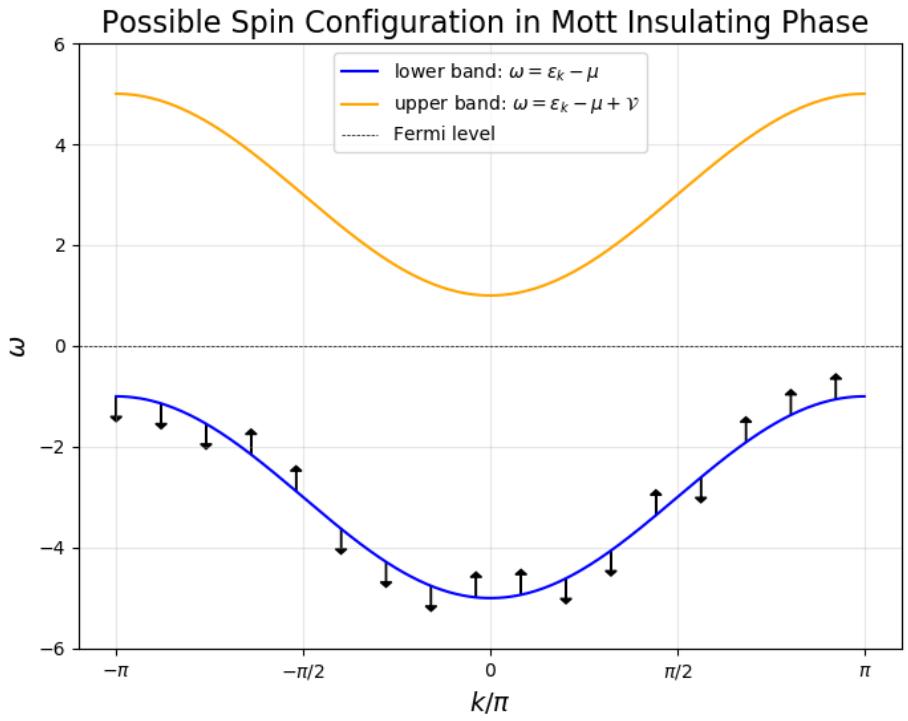

Figure 2.5: One of the 2^N configurations of the lower band being completely below the Fermi level, a Mott insulating phase. Spins are randomly distributed up or down

space. The system will be neither anti-ferromagnetic nor ferro-magnetic due to spin at each site being zero. As is with Ω_0 i.e. zero occupation.

In that regard we are particularly interested in the magnetization or average spin orientation of the HK model system in the relevant entropic state $k \in \Omega_1$ where spins can be either up or down in a randomly oriented fashion. We calculate that the magnetization per site is zero as expected. This can be shown by given that we have spin be defined by

$$\hat{S}_j = \hat{c}^\dagger_{j\alpha} \sigma_{\alpha,\alpha'} \hat{c}_{j\alpha'}. \tag{2.38}$$

Here α indicate spin indices and σ a Pauli matrix. To be able to calculate anything from our exactly solved model in momentum space we use the Fourier transform of the spin operator defined by

$$\hat{S}_q = \frac{1}{\sqrt{L}} \sum_j e^{iq \cdot r_j} \hat{S}_j. \tag{2.39}$$

Now in this expression we can write $\hat{S}_j$ equation (2.44) out in terms of momentum-dependent creation and annihilation operators defined by equations (2.5) and (2.6), such that we get

$$\hat{S}_q = \frac{1}{\sqrt{L}} \sum_j e^{iq\cdot r_j} \left[\frac{1}{\sqrt{L}} \sum_{k_1} e^{-ik_1\cdot r_j} \hat{c}^\dagger_{k_1,\alpha} \right] \sigma_{\alpha,\alpha'} \left[\frac{1}{\sqrt{L}} \sum_{k_2} e^{ik_2\cdot r_j} \hat{c}_{k_2,\alpha'} \right] \tag{2.40}$$

$$= \frac{1}{L^{3/2}} \sum_{j,k_1,k_2} e^{i(q-k_1+k_2)\cdot r_j} \hat{c}^\dagger_{k_1,\alpha} \sigma_{\alpha.\alpha'} \hat{c}_{k_2,\alpha'} \tag{2.41}$$

$$= \frac{1}{L^{3/2}} \sum_{k_1,k_2} \delta_{q-k_1+k_2=0} \hat{c}^\dagger_{k_1,\alpha} \sigma_{\alpha.\alpha'} \hat{c}_{k_2,\alpha'} \tag{2.42}$$

$$= \frac{1}{\sqrt{L}} \sum_k \hat{c}^\dagger_{k+q,\alpha} \sigma_{\alpha,\alpha'} \hat{c}_{k,\alpha'}. \tag{2.43}$$

So we write the coördinate space spin operator in momentum space k and transfer momentum q as

$$\hat{S}_j = \frac{1}{L} \sum_q e^{-iq\cdot r_j} \sum_k \hat{c}^\dagger_{k+q,\alpha} \sigma_{\alpha,\alpha'} \hat{c}_{k,\alpha'}. \tag{2.44}$$

.

Now we can calculate the average spin per site as

$$\langle \hat{S}^z_j \rangle = \frac{1}{L} \sum_q e^{-iq\cdot r_j} \sum_k \langle \hat{c}^\dagger_{k+q,\alpha} \sigma_{\alpha,\alpha'} \hat{c}_{k,\alpha'} \rangle \tag{2.45}$$

$$= \frac{1}{L} \sum_q e^{-iq\cdot r_j} \sum_k \left[\langle \hat{c}^\dagger_{k+q,\uparrow} \hat{c}_{k,\uparrow} \rangle - \langle \hat{c}^\dagger_{k+q,\downarrow} \hat{c}_{k,\downarrow} \rangle \right]. \tag{2.46}$$

$$\tag{2.47}$$

Here, creation and annihilation operators have to match in order to give non-zero contribution to the expectation value because of the orthogonality of eigenvectors in Hilbert space. Such that $\langle \hat{c}_{\uparrow k+q,\uparrow} \hat{c}_{k,\uparrow} \rangle$ only has contributions for $q = 0$. The expectation values in equation (2.52) will become number operators

$$\langle \hat{S}^z_j \rangle = \frac{1}{L} \sum_q e^{-iq\cdot r_j} \sum_k \left[\langle \hat{c}^\dagger_{k+q,\uparrow} \hat{c}_{k,\uparrow} \rangle - \langle \hat{c}^\dagger_{k+q,\downarrow} \hat{c}_{k,\downarrow} \rangle \right] \delta_{q=0} \tag{2.48}$$

$$= \frac{1}{L} \sum_k \left[\langle \hat{c}^\dagger_{k,\uparrow} \hat{c}_{k,\uparrow} \rangle - \langle \hat{c}^\dagger_{k,\downarrow} \hat{c}_{k,\downarrow} \rangle \right] \tag{2.49}$$

$$= \frac{1}{L} \sum_k \left[\langle ..., N_{k,\uparrow} - 1, ... | \sqrt{N_{k,\uparrow}} \sqrt{N_{k,\uparrow}} | ..., N_{k,\uparrow} - 1, ... \rangle - \langle ..., N_{k,\downarrow} - 1, ... | \sqrt{N_{k,\downarrow}} \sqrt{N_{k,\downarrow}} | ..., N_{k,\downarrow} - 1, ... \rangle \right] \tag{2.50}$$

$$= \frac{1}{L} \sum_k [N_{k,\uparrow} - N_{k,\downarrow}] \tag{2.51}$$

$$= 0. \tag{2.52}$$

Hence $\langle \hat{S}^z_j \rangle$vanishes, because there is no preference in spin orientation in the degenerate region $k \in \Omega_1$ i.e. $N_{k,\uparrow} = N_{k,\downarrow}$. For the other regions of occupancy where we have either $N_{k,\uparrow} = N_{k,\downarrow} = 0$ for $k \in \Omega_0$ trivially gives zero magnetization and for the, either way for $k \in \Omega_2$ we also find $N_{k,\uparrow} = N_{k,\downarrow}$ at every site in double occupancy region so no net magnetization over the whole system.

Now that we have calculated that the net magnetization is, maybe unsurprisingly zero, we can also investigate the spin correlation function between two sites. As this calculation results in a non-zero outcome for magnetic correlation this is a very interesting property of the HK model. Let us calculate the spin correlation function between two spin sites S_j and S_0 on the (one-dimensional) lattice, where we conveniently choose the spin at the origin S_0 and some at some site S_j, because then the Fourier transform translates to

$$\langle \hat{S}_j \hat{S}_0 \rangle = \frac{1}{L} \sum_q e^{-iq\cdot r_j} \langle \hat{S}_q \hat{S}_{-q} \rangle \tag{2.53}$$

$$= \frac{1}{L^2} \sum_q e^{-iq\cdot r_j} \sum_{k,k'} \left\langle \left(\hat{c}^\dagger_{k+q,\uparrow} \hat{c}_{k,\uparrow} - \hat{c}^\dagger_{k+q,\downarrow} \hat{c}_{k,\downarrow} \right) \left(\hat{c}^\dagger_{k'-q,\uparrow} \hat{c}_{k',\uparrow} - \hat{c}^\dagger_{k'-q,\downarrow} \hat{c}_{k',\downarrow} \right) \right\rangle . \tag{2.54}$$

$$\tag{2.55}$$

Looking at the first term, the expectation value $\langle \hat{c}^\dagger_{k+q,\uparrow} \hat{c}_{k,\uparrow} \hat{c}^\dagger_{k'-q,\uparrow} \hat{c}_{k',\uparrow} \rangle$ has now two non-zero contributions, $q = 0$ and $q = k' - k$ in order to let creation and annihilation operators match. Writing this out for this term gives us the following contributions to $\langle S_j S_0 \rangle$

$$\frac{1}{N^2} \sum_{q,k,k'} e^{-iq\cdot r_j} \langle \hat{c}^\dagger_{N+q,\uparrow} \hat{c}_{k,\uparrow} \hat{c}^\dagger_{k'-q,\uparrow} \hat{c}_{k',\uparrow} \rangle =$$

$$\frac{1}{N^2} \sum_{k,k'} \left[e^{-i(k'-k)\cdot r_j} \langle \hat{c}^\dagger_{k',\uparrow} \hat{c}_{k,\uparrow} \hat{c}^\dagger_{k,\uparrow} \hat{c}_{k',\uparrow} \rangle + \delta_{k'=k} \langle \hat{c}^\dagger_{k,\uparrow} \hat{c}_{k,\uparrow} \hat{c}^\dagger_{k',\uparrow} \hat{c}_{k',\uparrow} \rangle \right] =$$

$$\frac{1}{N^2} \sum_{k',k} \left[e^{-i(k'-k)\cdot r_j} N_{k',\uparrow} \langle \hat{c}_{k,\uparrow} \hat{c}^\dagger_{k,\uparrow} \rangle + N^2_{k,\uparrow} \right] =$$

$$\frac{1}{N^2} \sum_{k',k} \left[e^{-i(k'-k)\cdot r_j} N_{k',\uparrow} (1 - N_{k,\uparrow}) + N^2_{k,\uparrow} \right] =$$

$$\frac{1}{N^2} \left[\sum_{k'} e^{-ik'\cdot r_j} N_{k',\uparrow} \sum_k e^{ik\cdot r_j} - \sum_{k'} e^{-ik'\cdot r_j} N_{k',\downarrow} \sum_k e^{ik\cdot r_j} N_{k,\uparrow} + N^2_{k,\uparrow} \right] =$$

$$\frac{1}{N^2} \left[\delta_{r_j,0} N_{k',\uparrow} \delta_{r_j,0} - \delta_{r_j,0} N_{k',\uparrow} \delta_{r_j,0} N_{k,\uparrow} + N^2_{k,\uparrow} \right] \overset{r_j \neq 0}{=} 1. \tag{2.56}$$

For the cross term $\langle \hat{c}^\dagger_{k+q,\uparrow} \hat{c}_{k,\uparrow} \hat{c}^\dagger_{k'-q,\downarrow} \hat{c}_{k'\downarrow} \rangle$ we find it's only non-zero for $q = 0$. Because in that instance we retrieve

$$\frac{1}{N^2} \sum_{q,k,k'} e^{-iq\cdot r_j} \langle \hat{c}^\dagger_{k+q,\uparrow} \hat{c}_{k,\uparrow} \hat{c}^\dagger_{k'-q,\downarrow} \hat{c}_{k',\downarrow} \rangle = \frac{1}{L^2} \sum_{k,k'} \langle \hat{c}^\dagger_{k,\uparrow} \hat{c}_{k,\uparrow} \hat{c}^\dagger_{k',\downarrow} \hat{c}_{k',\downarrow} \rangle \tag{2.57}$$

$$= \frac{1}{N^2} \sum_{k,k'} \langle \hat{n}_{k,\uparrow} \hat{n}_{k'\downarrow} \rangle \tag{2.58}$$

$$= \frac{1}{N^2} \sum_{k,k'} \langle \hat{n}_{k,\uparrow} \rangle \langle \hat{n}_{k',\downarrow} \rangle \tag{2.59}$$

$$= \frac{1}{N^2} N_{k,\uparrow} N_{k',\downarrow} \tag{2.60}$$

$$= 1. \tag{2.61}$$

Given that we have $N_{k,\uparrow} = N_{k',\downarrow}$. Now we conclude $\langle S_j S_0 \rangle = \delta_{j,0}$ which shows that there is no long range order of any kind in the insulating phase.

2.5 Density of states and half-filling case

Now that we have a Green's function for our model, we want to examine for which conditions our system is in a half-filling state. In this situation half of the available states are occupied by an electron and the other half is empty, i.e., a particle-hole symmetry. To determine this we use the spectral-weight function, defined by the imaginary part of the Green's function

$$\rho_{\mathbf{k}\sigma}(\omega) = -\frac{1}{\pi} \Im[G^R_{\mathbf{k}\sigma}(\omega)], \tag{2.62}$$

with

$$\Im[G^R_{\mathbf{k}\sigma}(\omega)] = -\pi\left[(1-\langle\hat{n}_{k\sigma}\rangle\delta(\omega+\mu-\epsilon_k)+\hat{n}_{k\sigma}\delta(\omega+\mu-\epsilon_k-\mathcal{V})\right], \tag{2.63}$$

where we used that, $\Im[\frac{1}{x+i\eta}] = -\frac{\eta}{x^2+\eta^2}$ and, $\lim_{\eta\to 0}\frac{\eta}{x^2+\eta^2} = \pi\delta(x)$ to go from equation (10) to equation (6), where it should be remembered that $i0^+ = \lim_{\eta\to 0^+} i\eta$ approaching zero from above.

Now integrating the spectral-weight function up to the Fermi energy gives us the average number of occupation for a particular momentum k

$$\int_{-\infty}^{\mu} d\omega\rho_{\mathbf{k}\sigma}(\omega) = (1-\langle\hat{n}_{k\sigma}\rangle)\theta(\mu-\epsilon_k)+\langle\hat{n}_{k\sigma}\rangle\theta(\mu-\epsilon_k-\mathcal{V}) \equiv n_{\mathbf{k}\sigma} \tag{2.64}$$

where integrals over Dirac functions have become Heaviside step functions indicated by θ. This is due to the fact that we integrate up to the Fermi energy because we work at temperature $T = 0$ hence only occupied sites up to the Fermi energy $E_f = \mu$. Now to ensure half filling, we need enforce the condition that the expectation value of the number operator $\langle\hat{n}_{k\sigma}\rangle = 1/2$ and the total occupation number of $n_{\mathbf{k}\sigma} = \sum_k n_{\mathbf{k}\sigma} = 1/2$ at every k, giving

$$\sum_{k\in(-\pi,\pi)}\left(\frac{1}{2}\theta(\mu-\epsilon_k)+\frac{1}{2}\theta(\mu-\epsilon_k-\mathcal{V})\right) = \frac{1}{2} \tag{2.65}$$

yielding, that

$$\mu = \mathcal{V}/2 \tag{2.66}$$

is half filling.

2.6 Phase diagram

We construct a $T = 0$ phase diagram by considering the ground-state energies of the system calculated earlier in this chapter, these give rise to different energy bands given by lower and upper Hubbard bands mentioned in section 2.2. Depending on the value of the chemical potential μ and interaction potential $\mathcal{V}$ we have three different phases:

- metal phase, this phase corresponds to a state where electrons can freely move through a material due to available energy levels above the ground-state (Fermi) energy. This happens when the Fermi level ($\omega = 0$) crosses either one of the energy bands or both as depicted in Figure (2.4). There are always available sites in the lattice an electron can move to, which results in a current when a voltage is applied.

- 'conventional' band insulator, this phase corresponds to a state where no electrons can move through the material due to either a fully occupied lattice or a completely empty one. The Fermi energy lies completely above or below the energy bands. We use the term conventional because these type of insulators are perfectly described by conventional band theory which doesn't take into account electron interactions such as the Hubbard model or HK model.

- Mott insulator, when the system has one electron per site and there are no empty sites or double occupied sites there is enough 'room' for the electron to move to, but electron repulsion prevents electrons from hopping to different sites because they have to overcome a potential $\mathcal{V}$. This creates an energy gap in the excitation spectrum depicted in Figure (2.3). Here the Fermi energy lies between the lower and upper Hubbard bands. This gap arises when interaction $\mathcal{V}$ is high enough.

For a simple 1D disperstion $\epsilon_k = -2t\cos(k)$ we set up $\mu, \mathcal{V}$ phase diagram indicating metal, band insulator and Mott insulator phase. Having stated the definition of these phases we can derive lines that are boundaries between phases by considering that

- for $t = 1$ the metal phase is bounded by the maximum of the upper band and the minimum of the lower band. Lower band is bounded from below by Fermi energy that crosses $\min\{\epsilon_k-\mu\} = -2-\mu$ so $\mu = -2$, above it is bounded by the maximum of the upper band crossing $\omega = 0$ which is $\max\{\epsilon_k-\mu+\mathcal{V}\} = 0$ or $\mu = 2+\mathcal{V}$.

- In the same reasoning, Mott phase lies in between the two bands, such that it bounded by the lines $\max\{\epsilon_k - \mu\} = 0$ and $\min\{\epsilon_k - \mu + \mathcal{V}\} = 0$ which corresponds to $\mu = 2$ and $\mu = -2 + \mathcal{V}$.
- Band insulator for $\mu > 2 + \mathcal{V}$ and $\mu < -2$. Fully occupied sites or zero occupation.

As stated earlier in section 2.3, due to lack of spin alignment we have a degenerate ground-state. The value of the entropy in the ground-state can be calculated because we know entropy $S = \ln(\Omega)$ with Ω the amount of micro states here related to the different spin directions which gives $\Omega = 2$, up or down spin. Then the entropy can be retrieved from the phase diagram identifying how large the region of single occupation is, $k \in \Omega_1$ is for every μ and $\mathcal{V}$. This corresponds to an entropy of $S = n_1 \ln(2)$ where n_1 is the number of particles in Ω_1. See Figure (2.6) for the different phases and corresponding entropy.

Remark the black dashed lines where the excitation energies are set to zero i.e. $\xi_k = 0$ and $2\xi_k + V = 0$. Here we see an increase in number of singly occupied states and corresponding to that an entropy due to the degeneracy of ground-state in that part of the phase diagram. It is here where one of the energy bands touch/(are tangent to) the Fermi surface. Which means there is one point for which it equals the Fermi level. When in the metal phase this means that in this instance we only have 2 possible occupations, either only $k \in \Omega_1$ and $k \in \Omega_2$ or we have only $k \in \Omega_0$ and $k \in \Omega_1$, but not all three possibilities. This increased spikes in entropy marks the boundaries of regions in metal phase for which we have

- Ω_0 and Ω_1 in the I region
- Ω_0 and Ω_2 in the II region
- Ω_0, Ω_1 and Ω_2 in the III region.

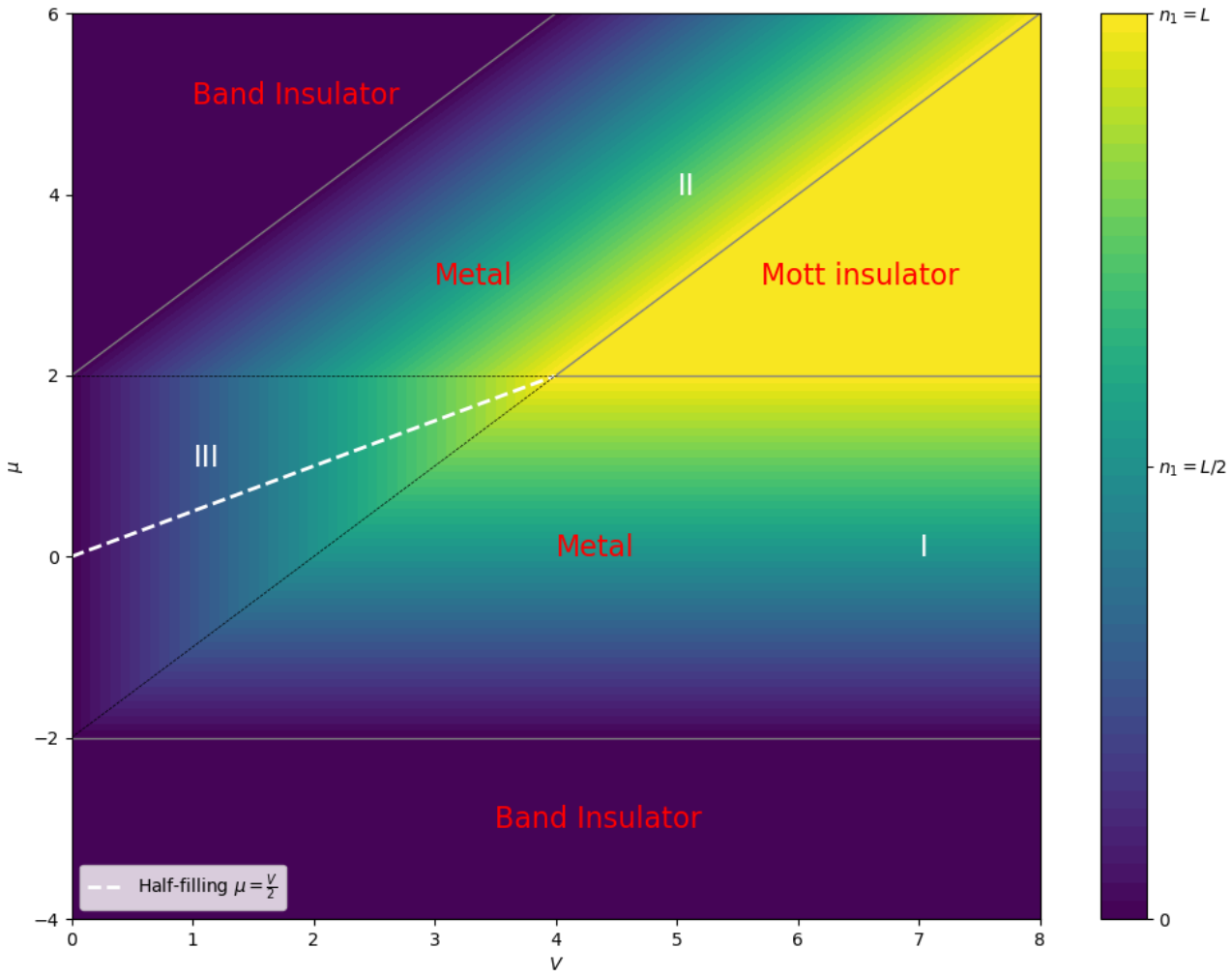

Figure 2.6: Different phases are indicated. Blue region: band insulator, schaded region: metal and the yellow region: Mott insulator. The color bar represents how large the region of single occupation, i.e., with entropy is. This is maximal for the length of the lattice L.

Chapter 3

Fermi surfaces and pseudogaps

To start with the introduction of the concept of Fermi arcs we first look into a model proposed by Kun Yung et al. [19], that gives a very simple description of disconnected regions in the Fermi surface and how they very naturally arise from the Hatsugai-Kohmoto model when we make a modification in the interaction. First we explain what Fermi surfaces are and their connection with the Luttinger sum rule, a fundamental theorem that is important for correlated-electron models.

3.1 Fermi surface and Luttinger sum rule

Given the Pauli exclusion principle, Fermions take up only allowed energy levels up to the Fermi level in the ground-state as we mentioned in the previous chapter. Considering we would have a system of N non-interacting fermions in volume V, the allowed energy levels of $2s+1$ states of energy, where s is spin quantum number, is the sum over all possible momentum up to the Fermi momentum p_F

$$N = \frac{(2s+1)V}{h^3} \int_{p \leq p_F} d^3p = \frac{(2s+1)V}{h^3} \frac{4\pi}{3} p_F^3, \tag{3.1}$$

such that the Fermi momentum is given by

$$p_F = \left(\frac{6\pi^2}{2s+1} \right)^{1/3} \hbar n^{1/3}, \tag{3.2}$$

where $\frac{N}{V} = n$. The sphere of the radius of this Fermi momentum p_F is called the Fermi sphere and it's surface is the Fermi surface. In solid-state physics and correlated electron models this Fermi surface is much more complicated than a simple spherical surface and determined by symmetries in a crystal lattice. The HK model with it's simple two-band structure in momentum space (barely more complicated that the this non-interacting regime) can however be good starting point for investigating fermi surfaces of otherwise hard to tackle quantum-many calculations in cuprates given that we have (three) exact ground-states in each k.

Given the HK model and its ground-state energies, we can retrieve the Fermi surface by identifying the lowest possible ground-states in k space. For a simple 2d dispersion we use

$$\epsilon_k = -2t \left(\cos(k_x) + \cos(k_y) \right), \tag{3.3}$$

and we use short hand notation $\xi_k = \epsilon_k - \mu$. Considering the three different ground-state energies and their number occupation from the previous chapter we have two Fermi surfaces for the points in k for which

- $\xi_k = 0$ i.e. the lower Hubbard band crossing the Fermi level
- $\xi_k + \mathcal{V} = 0$ i.e. the upper Hubbard band crossing the Fermi level

This results in two Fermi surfaces given by Figure (3.1). As can be seen, two closed curves appear. Now, Luttinger theorem [9] also known as Luttinger sum rule states that the number of particles is directly related to volume enclosed by the Fermi surface. In general this statement translates to

$$2\int_{\Re G(k,\omega=0)>0}\frac{d^3k}{(2\pi)^3}=\frac{N}{V}. \tag{3.4}$$

For a number of N particles in a volume enclosed by the Fermi surface of V. This is a very general result and logically applies to systems of non-interacting fermions, but it turns out it applies to system with interactions as well, except for superconducting states and Cooper pairing. In normal Fermi liquids this means that Fermi surfaces always should be closed.

We can also write the Luttinger sum rule or Luttinger count as

$$n = 2\sum_{k}\Theta(\Re G_{k\sigma}(\omega=0)) \tag{3.5}$$

$$= 2\sum_{k\in\Omega_1}\Theta(\Re G_{k\sigma}(\omega=0)+\sum_{k\in\Omega_2}\Theta(\Re G_{k\sigma}(\omega=0) \tag{3.6}$$

where Θ is the Heaviside step function. In our case the Green's function (for the first term in equation (3.6) consist of two terms and zeros. Except for special cases where $\mu = \mathcal{V}/2$, i.e., particle-hole symmetry or $\mathcal{V} = 0$ (model is non-interaction) Luttinger's sum rule is violated in the HK model [14]. This is because the requirement $\Re G_{k\sigma}(\omega = 0) > 0$ is obtained by poles and zeros such that they enter the particle density on the same footing[3]. Therefore the Luttinger count doesn't match the occupancy. The single occupied region Ω_1 contributes if it where fully occupied when the zeros go above the chemical potential.

How a violation of Luttinger's theorem through the appearance of zeros in the Green's function results in the formation of disconnected Fermi surfaces will be explained in the next section.

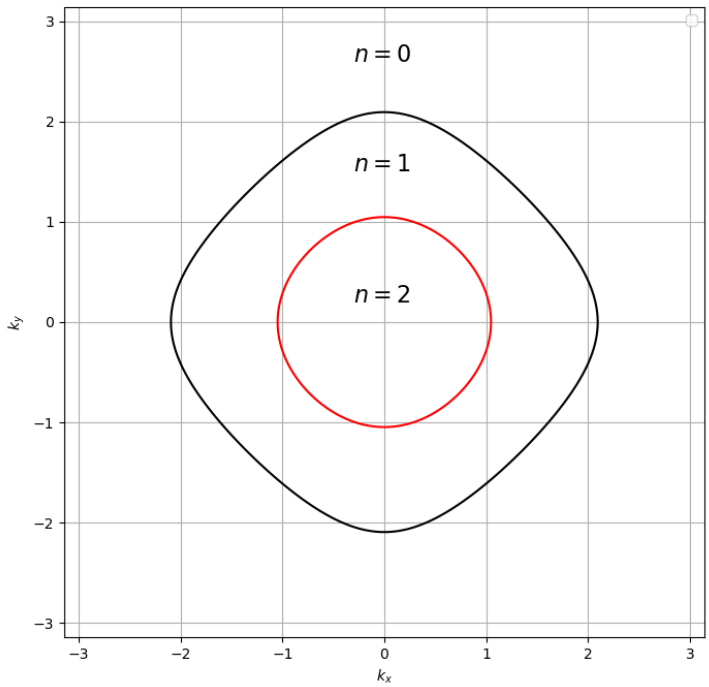

Figure 3.1: Two Fermi surfaces for the lower Hubbard band (black) and upper Hubbard band (red) for $\mu = -1$ and $\mathcal{V} = 2$. They are boundaries of different occupation number, inside the red: n=2, between black en red: n=1, outside black: n=0

3.2 Pseudogaps

For a very natural understanding of pseudogaps in the Fermi surface we can use a model which is a slight deviation from the HK model. In this model the Hamiltonian is given by

$$H = \sum_k \left[(\epsilon_k - \mu)(\hat{n}_{k,\uparrow} + \hat{n}_{k,\downarrow}) + U_k \hat{n}_{k,\uparrow} \hat{n}_{k,\downarrow} \right], \tag{3.7}$$

where we use a 2D dispersion, but anisotropic such that

$$\epsilon_k = -2t_x \cos(k_x) - 2t_y \cos(k_y), \tag{3.8}$$

with hopping parameters t_x and t_y in the x and y direction respectively. Following the reasoning of [19] we then purely for heuristic reasons introduce a new interaction potential U_k in which we add to the non-local interaction U with a k-dependency, such that we have

$$U_k = -2T_x \cos(k_x) - 2T_y \cos(k_y) + U, \tag{3.9}$$

where T_x and T_y can be understood as hopping parameters in the x and y direction of the center of mass of two interacting fermions[19]. Details of how this interaction is formed are not important for this discussion, it is merely to understand how a violation of Luttinger's theorem can occur in the context of a Green's function with zeros.

Given that we now have an interaction U_k which can change between being positive or negative, we have a different occupation pattern in the ground-state. Contrary to the case where $U_k = \mathcal{V}$ our normal HK model, we now have a situation where the two Fermi surfaces as depicted in Figure (3.2) can cross due to changing behavior of U_k in k space. Because of the possibility of U_k being negative we need to consider different conditions for the ground-state occupation pattern. If $0 < \xi_k$ it not only suffices as the condition for zero occupation $n = 0$ as in the $U_k = \mathcal{V}$ case but we also need the eigenenergy $2\xi_k + U_k > 0$ to be higher than zero because U_k is not necessarily positive for every k. Also, for double occupation $n = 2$, $\xi_k + U_k < 0$ not only suffices as a condition but we also need $2\xi_k + U_k < 0$. This gives us an occupation pattern described by

- n=0 for $\xi_k > 0$ and $2\xi_k + U_k > 0$
- n=1 for $\xi_k < 0$ and $\xi_k + U_k < 0$
- n=2 for $\xi_k + U_k < 0$ and $2\xi_k + U_k < 0$.

As can be seen in figure (3.2), we see next to the normal Fermi surfaces (red and black lines) which we got from the HK model with constant potential $\mathcal{V}$ also that a new kind of Fermi surface appears which acts as the boundary between the zero $n = 0$ and double $n = 2$ occupations (blue line). This surface defined by the solution to $2\xi_k + U_k = 0$ can be denoted as "pseudo" Fermi surface. Pseudo because it does not represent the excitations energies of the Green's function when they cross the Fermi level, but it represents those points where the Green's function $G(k, \omega = 0) = 0$, i.e., the zeros as depicted in figure (2.4) passing through the Fermi level $\omega = 0$. Indeed, $2\xi_k + U_k = 0$ or $\xi_k + U_k/2 = 0$ are those points in the excitation spectrum where the two terms in the Green's function cancel each other out at equal weight, i.e., $\omega = \xi_k + U_k/2$ are actually those energies where the fermions are gapped with a gap $U_k/2$, hence the name pseudo gap. Where the disconnected Fermi surfaces (black en red) or Fermi arcs now represents poles at $\omega = 0$ of the Green's function the pseudo Fermi surface represents the zeros at $\omega = 0$. Like the real Fermi surface the Green's function $G(k, \omega = 0)$ changes sign at the pseudo Fermi surface but now it does so smoothly, because $G(k, \omega = 0)$ itself is zero at those points.

In principle Luttinger sum rule is violated because it states that Fermi surfaces should always be closed. However Fermi arc plus pseudo Fermi surface is still closed, it's becoming clear that we are not working with a Fermi-liquid here.

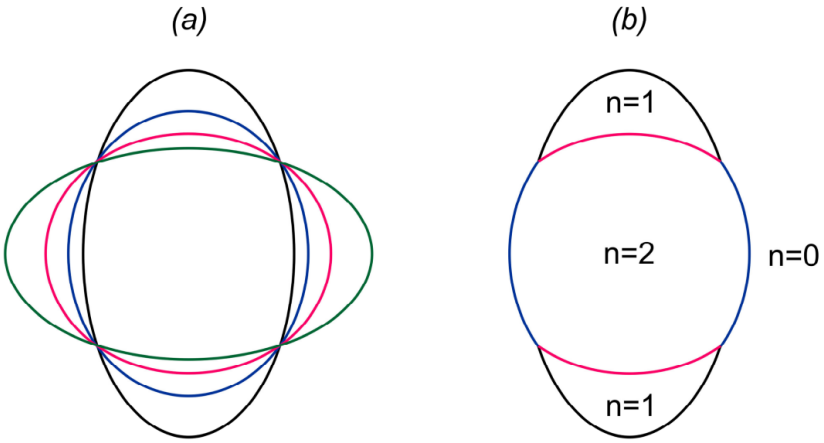

Figure 3.2: Solutions to: $\xi_k = 0$ (black lines), $\xi_k + U_k = 0$ (red lines), $2\xi_k + U_k = 0$ (blue lines) and $U_k = 0$ (green line) (a). Occupation pattern in the ground-state, red and black lines are Fermi surfaces. Blue line is pseudo Fermi surface (b). Taken from [19]

Chapter 4

Spin coupling and Fermi arcs

Having established the Hatsugai-Kohmoto model to understand the pseudogap regime in cuprates, we have the ingredients to investigate a newly discovered model by Worm et al.[18]. In the previous section we saw how a momentum-dependent interaction as a modification in the HK model can give rise to Fermi arcs and pseudo gaps, but this was done very hand-wavingly. In this chapter we introduce a momentum-dependent interaction which actually couples different points in the Brillouin zone separated by a transfer momentum Q, such that disconnected Fermi arcs emerge out of the antiferromagnetic spin fluctuation in momentum-space.

4.1 Eigenstates and Green's function

First, the Hamiltonian is[18]

$$H = \sum_{\mathbf{k}\sigma} \left[(\epsilon_{\mathbf{k}} - \mu)\hat{n}_{\mathbf{k}\sigma} + \frac{\mathcal{V}}{2}\hat{n}_{\mathbf{k}\sigma}\hat{n}_{\mathbf{k}+\mathbf{Q}-\sigma} \right]. \tag{4.1}$$

In this Hamiltonian we introduced a momentum transfer $\mathbf{Q} = (\pi, \pi)$ in the HK model, which couples fluctuating spins on different momenta, making the interaction momentum-dependent. The Green's function of the system is again easily calculated considering we have four eigenstates. These are given by

- $|0\rangle$ i.e. the vaccuum state
- $\hat{c}^\dagger_{k,\sigma}|0\rangle = |k,\sigma\rangle$ one electron at momentum k with spin σ
- $\hat{c}^\dagger_{k+Q,\sigma}|0\rangle = |k+Q,\sigma\rangle$ one electron at momentum $k+Q$ with spin σ
- $\hat{c}^\dagger_{k,\sigma}\hat{c}^\dagger_{k+Q,\sigma}|0\rangle = |k,\sigma;k+Q,-\sigma\rangle$ one electron at k and one at $k+Q$ with opposite spin σ and $-\sigma$.

The corresponding eigenenergies of these eigenstates are

- $E_0 = 0$ for the $|0\rangle$ state
- $E_k = \xi_k$ for the $|k,\sigma\rangle$ state
- $E_{k+Q} = \xi_{k+Q}$ for the $|k+Q,\sigma\rangle$ state
- $E_{k,k+Q} = \xi_k + \xi_{k+Q} + \mathcal{V}$ for the $|k,\sigma;k+Q,-\sigma\rangle$ state

Now, for computing the Green's function we follow the procedure described in section 2.2. There, we can take off from equation (2.28)

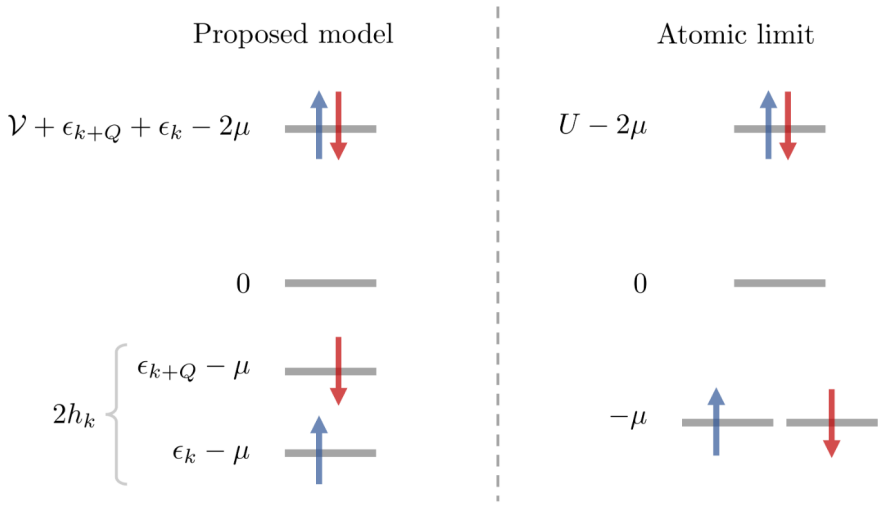

Figure 4.1: Schematic overview of eigen states in the given model. As comparison the atomic limit ($\epsilon_k = 0$) is given. Here the proposed model can be seen as a set of atomic limit models with in the presence of a magnetic field $h_k = (\epsilon_k - \epsilon_{k+Q})/2$. Taken from [4].

$$G^R_{k\sigma}(t) = -i\theta(t)\frac{1}{Z}\sum_{n,m}(e^{-\beta E_n} + e^{-\beta E_m})e^{it(E_n - E_m)} \langle n|\hat{c}_{\mathbf{k}\sigma}|m\rangle \langle m|\hat{c}^\dagger_{\mathbf{k}\sigma}|n\rangle \tag{4.2}$$

$$= -i\theta(t)\frac{1}{Z}\sum_{n,m}(e^{-\beta E_n} + e^{-\beta E_m})e^{it(E_n - E_m)} |\langle m|\hat{c}^\dagger_{\mathbf{k}\sigma}|n\rangle|^2, \tag{4.3}$$

Where we used that $\langle n|\hat{c}_{k,\sigma}|m\rangle = \langle m|\hat{c}^\dagger_{k,\sigma}|n\rangle^*$. Here, the summation is over all possible eigenstates n, m that we described. Considering that $G^R_{k\sigma}$ contains creation/annihilation operators at momentum k, we can check for every combination of n and m and look which ones do not give zero in the overlap integral $\langle m|\hat{c}^\dagger_{\mathbf{k}\sigma}|n\rangle$. It turns the only non-zero overlap integrals are: $\langle k,\sigma|\hat{c}^\dagger_{\mathbf{k}\sigma}|0\rangle = \langle k,\sigma|k,\sigma\rangle = 1$, and $\langle k,\sigma;k+Q,-\sigma|\hat{c}^\dagger_{\mathbf{k}\sigma}|k+Q,-\sigma\rangle = \langle k,\sigma;k+Q,-\sigma|k,\sigma;k+Q,-\sigma\rangle = 1$. This comes down to the following combinations for n and m

- $m = |k,\sigma\rangle$ and $n = |0\rangle$, with $E_m = \xi_k$ and $E_n = 0$
- $m = |k,\sigma;k+Q,-\sigma\rangle$ and $n = |k+Q,-\sigma\rangle$, with $E_m = \xi_k + \xi_{k+q} + \mathcal{V}$ and $E_n = \xi_{k+Q}$.

Plugging these two combinations of states with the corresponding eigenenergies into equation (2.60), we retrieve a Green's function consisting of two terms

$$G^R_{k\sigma}(t) = -i\theta(t)\frac{1}{Z}\left[(e^{-\beta 0} + e^{-\beta\xi_k})e^{it(0-\xi_k)} + (e^{-\beta\xi_{k+Q}} + e^{-\beta(\xi_k+\xi_{k+Q}+\mathcal{V})})e^{it(\xi_{k+Q}-\xi_k-\xi_{k+Q}-\mathcal{V})}\right] \tag{4.4}$$

$$= -i\theta(t)\frac{1}{Z}\left[(1 + e^{-\beta\xi_k})e^{-it\xi_k} + (e^{-\beta\xi_{k+Q}} + e^{-\beta(\xi_k+\xi_{k+Q}+\mathcal{V})})e^{-it(\xi_k+\mathcal{V})}\right] \tag{4.5}$$

$$= -i\theta(t)\left[(1 - n_{\mathbf{k}+\mathbf{Q}})e^{-it\xi_k} + n_{\mathbf{k}+\mathbf{Q}}e^{-it(\xi_k+\mathcal{V})}\right], \tag{4.6}$$

where

$$\hat{n}_{\mathbf{k}+\mathbf{Q}} = \frac{e^{-\beta\xi_{\mathbf{k}+\mathbf{Q}}} + e^{-\beta(\xi_{\mathbf{k}}+\xi_{\mathbf{k}+\mathbf{Q}}+\mathcal{V})}}{Z} \tag{4.7}$$

is the expectation value of the number operator, $\hat{n}_{\mathbf{k}+\mathbf{Q}} = \langle\hat{n}_{\mathbf{k}+\mathbf{Q}\sigma}\rangle$ of electrons situated at momentum $\mathbf{k}+\mathbf{Q}$ with spin σ. Taking a Fourier transform of equation (3.6) we get

$$G_{\mathbf{k}\sigma}(\omega) = \frac{1 - \hat{n}_{\mathbf{k}+\mathbf{Q}}}{\omega + \mu - \epsilon_k + i0^+} + \frac{\hat{n}_{\mathbf{k}+\mathbf{Q}}}{\omega + \mu - \epsilon_k - \mathcal{V} + i0^+}. \tag{4.8}$$

4.2 Occupation of the ground-state in momentum space

Following the reasoning from chapter 3, the ground-state occupation pattern can be retrieved from looking where in momentum space, which eigenstate with corresponding eigenenergy is minimized with respect to other possible ground-state eigenenergies. Here the ground-state occupation is more complicated so we go over the requirements of each region in more detail with it's corresponding occupation numbers. For a given chemical potential and interaction potential $\mu = -0.3$ and $\mathcal{V} = 1.5$ we can divide regions in momentum space by different ground-energies and their occupations. We use $\xi_k = \epsilon_k - \mu$. And we use a dispersion including next-(to next-)nearest neighbors of (see appendix B)

$$\epsilon_k = -2t(\cos(k_x) + \cos(k_y)) - 4t' \cos(k_x)\cos(k_y) - 2t''(\cos(2k_x) + \cos(2k_y)), \tag{4.9}$$

where $t = 1$, $t' = -0.2$ and t" $= 0.1$ are typical values found in low-energy tight-binding models for cuprates[12]. In this dispersion relation there is accounted for next-(to next-)nearest neighbors, given by the terms with parameters t' and t'' respectively.

As we described in section 1, we either have a ground-state energy of $E_{gs} = \xi_k$ for state $|k, \sigma\rangle$, $E_{gs} = \xi_{k+Q}$ for state $|k + Q, \sigma\rangle$, $E_{gs} = \xi_k + \xi_{k+Q} + \mathcal{V}$ for state $|k, \sigma; k + Q, -\sigma\rangle$ and $E_{gs} = \xi_k + \xi_{k+Q}$ for $|k, \sigma; k + Q, \sigma\rangle$ (where the last corresponds to double occupation but no antiferromagnetic spin coupling and no interaction potential $\mathcal{V}$ between the electrons).

First for the state where an electron is positioned at momentum k with a spin σ, $|k, \sigma\rangle$ and has ground-state energy of $E_{gs} = \xi_k$. That means that an electron is found in this region of k space but non on $k + Q$ hence no coupling of different momenta and a single occupied state without interaction. Let ξ_k be the lowest of all ground-state energies of the system and we have single-occupied state. This is given for the following conditions for k

- $\xi_k < 0$,
- $\xi_k < \xi_{k+Q}$,
- $\xi_k < \xi_k + \xi_{k+Q}$, gives $\xi_{k+Q} > 0$,
- $\xi_k < \xi_k + \xi_{k+Q} + \mathcal{V}$, gives $\xi_{k+Q} + \mathcal{V} > 0$,
- $\xi_{k+Q} < \xi_k + \xi_{k+Q} + \mathcal{V}$, gives $\xi_k + \mathcal{V} > 0$. This ensures that we exclude the values of k for which coupling of opposite spins occur. Meaning that for an electron positioned on k the energy of the electron positioned at $k + Q$ should be lower than the ground-state energy with AF coupling.

This region of for this occupation is given in Figure (4.2 (1)).

From a state $|k, \sigma\rangle$ we can move to a point in momentum space separated by $Q = (\pi, \pi)$ such that we have the new state $|k + Q, \sigma\rangle$. This can be viewed as a single occupied state as it has a ground-state energy of $E_{gs} = \xi_{k+Q}$. However this energy refers to occupation of $|k, \sigma\rangle$. Hence the region corresponding to the energy $E_{gs} = \xi_{k+Q}$ has no electron positioned on these points in k space. The region corresponding to $E_{gs} = \xi_{k+Q}$ is governed by

- $\xi_{k+Q} < 0$,
- $\xi_{k+Q} < \xi_k$,
- $\xi_{k+Q} < \xi_k + \xi_{k+Q}$, gives $\xi_k > 0$,
- $\xi_{k+Q} < \xi_k + \xi_{k+Q} + \mathcal{V}$, gives $\xi_k + V > 0$
- $\xi_k < \xi_k + \xi_{k+Q} + \mathcal{V}$, gives $\xi_{k+Q} + V > 0$. Again excluding the values of $k + Q$ for which there is a coupling with electron with momenta k with opposite spin.

In this region the ground-state energy is $E_{gs} = \xi_{k+Q}$, but there are no electrons in this regions. The electrons positioned at momentum k yield an energy of ξ_{k+Q} on momentum $k + Q$ but we find a

vacuum in this region. $|k+Q,\sigma\rangle$ state is indicated in Figure (4.2 (2)) .

For double occupation without coupling given by the state $|k,\sigma;k+Q,\sigma\rangle$. This holds if we find an electron positioned at k and also at $k+Q$ but their spin is equal such that there is no interaction via coupling. Ground-state energy in this region of momentum space is given by $E_{gs}=\xi_k+\xi_{k+Q}$. This holds for the conditions:

- $\xi_k+\xi_{k+Q}<\xi_k$, or $\xi_{k+Q}<0$,
- $\xi_k+\xi_{k+Q}<\xi_{k+Q}$ or $\xi_k<0$,
- $\xi_k+\xi_{k+Q}<0$.

Given in Figure (4.2(3)).

A zero occupied state with zero energy $E_{gs}=0$, given by $|0\rangle$ is located for momenta k for which this ground-state energy is the lowest

- $0<\xi_k$,
- $0<\xi_{k+Q}$.

Given in Figure (4.2 (4)).

A double occupied state $|k,\sigma;k+Q,-\sigma\rangle$ holds if an electron is positioned on k with a given spin σ and there is an electron on $k+Q$ with opposite spin $-\sigma$. We find for the region correpsonding to this ground-state that the energy $E_{gs}=\xi_k+\xi_{k+Q}+\mathcal{V}$ should be lowest of all possible eigenenergies. This is the case for

- either $\xi_k+\xi_{k+Q}+\mathcal{V}<\xi_k$,
- or $\xi_k+\xi_{k+Q}+\mathcal{V}<\xi_{k+Q}$.

The region of double occupation k and $k+Q$ with (opposite) spin coupling is depicted in Figure (4.3)

Considering all ground-state occupations and their energies we find that, different regions of occupation are divided by solutions to

- $\xi_k=0$,
- $\xi_{k+Q}=0$,
- $\xi_k+\mathcal{V}=0$,
- $\xi_{k+Q}+\mathcal{V}=0$.

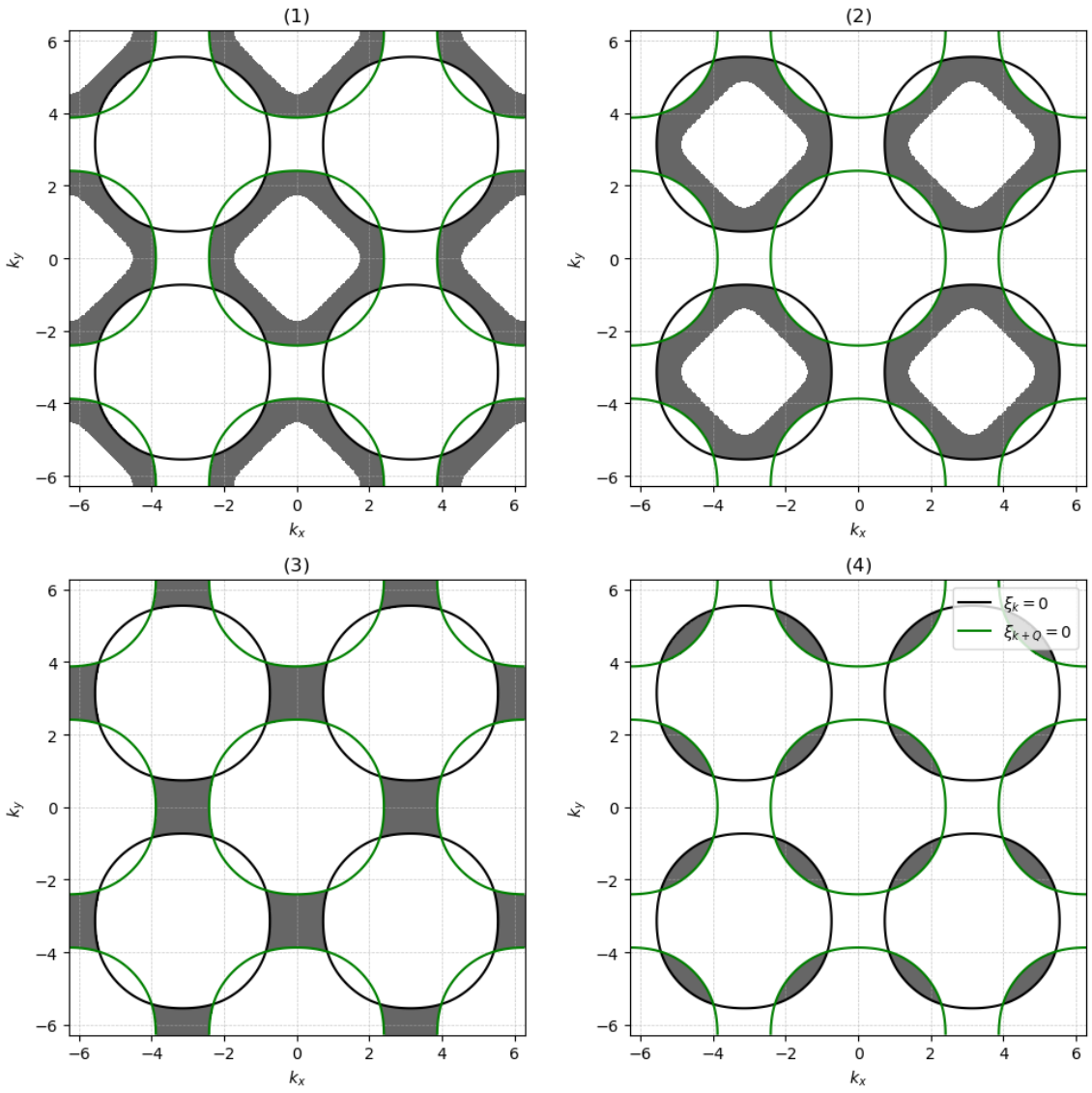

Figure 4.2: Ground-state occupation pattern in two Brillouien zones: Indicated in the gray areas are states $|k,\sigma\rangle$ (1), $|k+Q,\sigma\rangle$ (2), $|k,\sigma;k+Q,\sigma\rangle$ (3) and $|0\rangle$ (4). Solutions to $\xi_k = 0$ (Fermi surface) and $\xi_{k+Q} = 0$ are given black and green curves respectively. This occupation pattern corresponds to $\mu = -0.3$ and $\mathcal{V} = 1.5$. Here we took $T = 10^{-2}$ i.e. low temperature limit for ground-state occupations.

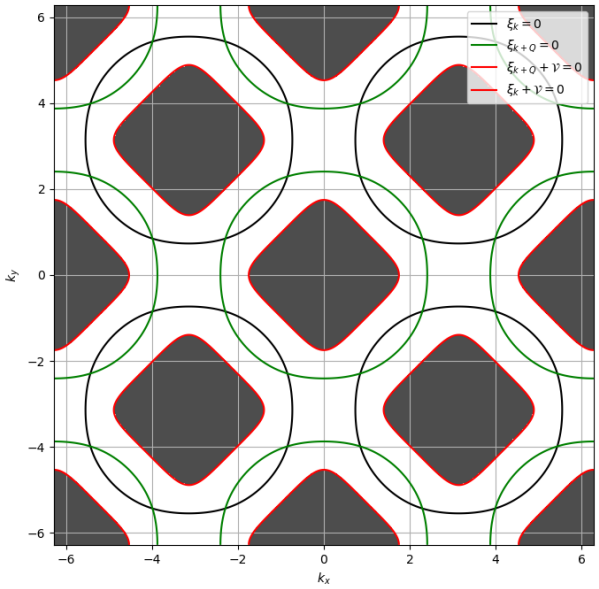

Figure 4.3: Regions for double occupation with opposite spin coupling, $|k, \sigma; k+Q, -\sigma\rangle$ are indicated in gray. Solution to $\xi_k + \mathcal{V} = 0$ (shifted Fermi surface) and $\xi_{k+Q} + \mathcal{V} = 0$ are given by the red curves. We use the same parameters for μ and $\mathcal{V}$ as Figure (4.2).

4.3 Formation of nodal Fermi arcs

The two pole structure of the Green's function we derived in equation (4.8), indicates the possibility of zeros as we described in section 2.3. Here the zeros are given by resolving the Green's function equation (4.8) for the condition $G_{k\sigma}(\omega = 0) = 0$, giving us the following relation for the Luttinger surface: $\xi_k - (\hat{\mathbf{n}}_{\mathbf{k}+Q} - 1)\mathcal{V} = 0$. Solutions to this equation are points in k where the Green's function is zero such that the electron excitation energy will be zero at those points. This can be seen by plugging $\omega = \xi_k - (\hat{n}_{\mathbf{k}+Q} - 1)\mathcal{V}$ in equation (4.8).

Now in the section 4.1 we calculated $\hat{n}_{\mathbf{k+Q}}$. The value of this average value of the number operator $\langle \hat{n}_{\mathbf{k+Q},\sigma} \rangle$ is in the zero temperature limit $T \to 0$ either $\hat{n}_{\mathbf{k+Q}} = 0$ when an electron on $\mathbf{k}$ is coupled via $\mathbf{Q}$ to an empty states. We calculated the occupation numbers by identifying lowest eigen-energies in each part of the Brillouin zone. We remark that states $|k, \sigma\rangle$ are coupled to empty states on position $\mathbf{k} + \mathbf{Q}$ therefore $\hat{n}_{\mathbf{k+Q}} = 0$ there. On the other hand the empty state $|k + Q, \sigma\rangle$ is coupled to filled states on $\mathbf{k}$ therefore $\hat{n}_{\mathbf{k+Q}} = 1$ in the region corresponding to that state.

Now depending on the value of $\hat{\mathbf{n}}_{\mathbf{k+Q}}$ the Luttinger surface can either overlap the non-shifted Fermi surface given by $\xi_k = 0$ or the shifted Fermi surface with interaction $\xi_k + \mathcal{V} = 0$ when $\hat{\mathbf{n}}_{\mathbf{k+Q}} = 1$ or $\hat{\mathbf{n}}_{\mathbf{k+Q}} = 0$ respectively. Because we choose the transfer momentum $Q = (\pi, \pi)$ the lines separating the $\hat{\mathbf{n}}_{\mathbf{k+Q}} = 0$ and $\hat{\mathbf{n}}_{\mathbf{k+Q}} = 1$ region is exactly $\pm k_x \pm k_y = \pi$ we call this the the antiferromagnetic zone boundary (AFZB), because in this region k couples via transfer momentum Q to states with $\hat{\mathbf{n}}_{\mathbf{k+Q}} = 0$ such that the (non-interacting) Fermi surface defined by solutions to $\xi_k = 0$ remains intact as can be seen in Figure (4.4). In the same manner, points outside the AFZB couple to filled states such that $\hat{\mathbf{n}}_{\mathbf{k+Q}} = 1$. That way the (interacting/shifted) Fermi surface defined by solution to $\xi_k + \mathcal{V} = 0$ vanishes when it comes outside the AFZB. This can been seen by increasing chemical potential such that parts of this (interacting) Fermi surface lie outside the AFZB, those parts are now intact an we have an anti-nodal Fermi arc.

How nodal and anti-nodal Fermi arcs transition into one each can be seen in the a phase diagram in Figure (4.6). Depending on the value of $\mathcal{V}$ and μ we have either electron-like Fermi surface corre-

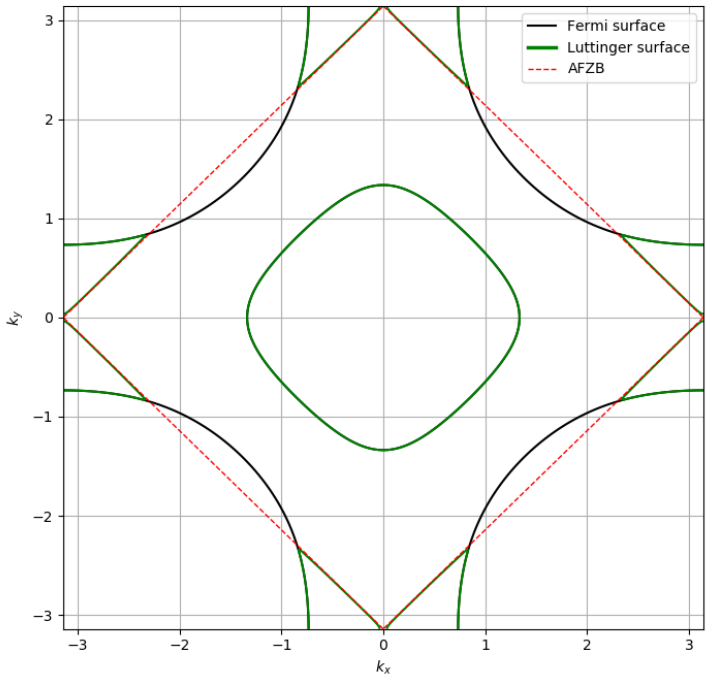

Figure 4.4: Nodal Fermi arcs through momentum coupling in number operator $\hat{\mathbf{n}}_{k+Q}$. In red the lines $\pm k_x \pm k_y = \pi$ corresponding to antiferromagnetic zone boundary (AFZB). Here $\mu = -0.3$ and $\mathcal{V} = 1.5$.

sponding to a non-interacting Fermi surface inside the AFZB or hole-like Fermi surface corresponding to the an interacting Fermi surface fully outside the AFZB. A gapped region corresponds to $\xi_k = 0$ Fermi surface fully outside the AFZB and $\xi_k + \mathcal{V} = 0$ inside the AFZB. Here the lines separating the different regimes of different kind of arcs and gaps given by the black and blue dashed and solid lines are retrieved from considering boundary point $(\pm\pi, 0)$,$(0, \pm\pi)$ and $(\pm\pi/2, \pm\pi/2)$ in dispersion ϵ_k. In Figure (4.7) we plotted the $\hat{n}_{\mathbf{k},\sigma}$ and $\hat{n}_{\mathbf{k},-\sigma}$. Plotting them both in the same picture we get the same regions in k space for either double, single and zero occupation as we got from inspecting all ground-state energies. In Figure (4.7) we also see the Fermi arcs and Luttinger arcs in two Brillouin zones. Remark that a connected surfaces appears consisting of Fermi arcs plus Luttinger arcs which is closed and has the same shape as the fully connected Fermi surfaces we would get if we considered the non-coupled interaction $\hat{H}_{interaction} = \frac{1}{2}\mathcal{V}\hat{n}_{\mathbf{k},\sigma}\hat{n}_{\mathbf{k},-\sigma}$(HK model). This connected surface consisting of Luttinger arcs and Fermi arcs now encloses an area in k space which consists of three different ground-state energy regions with corresponding occupation number, as can be seen in Figure (4.7) and in Figure (4.2) and (4.3) relating the different regions of occupation to their given eigenstates.

The location of Fermi arcs given by Figure (4.4) in the nodal direction agrees with APRES expemirents on cuprates as for example performed on $YBa_2Cu_3O_{7-\delta}$ [6] and APRES experiments on $Bi_2Sr_2CaCu_20_{8+\delta}$ [17].

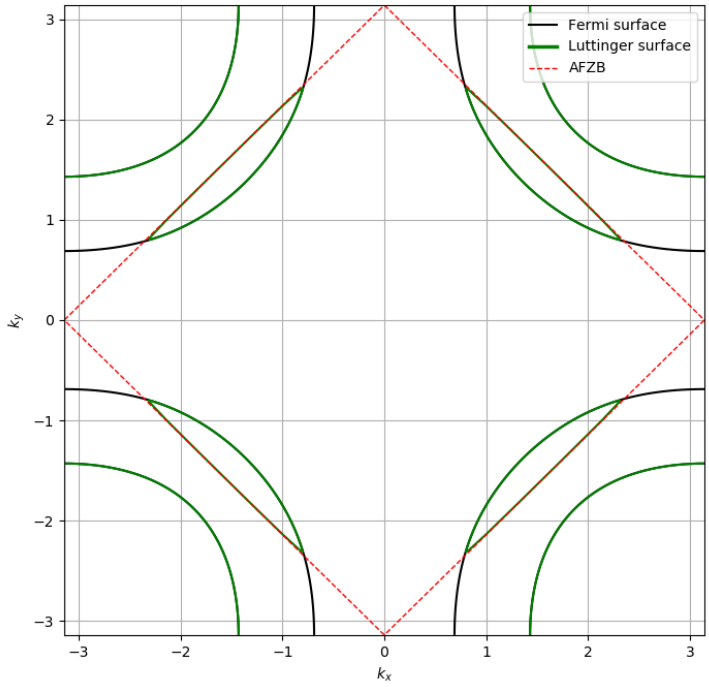

Figure 4.5: Anti-nodal Fermi arcs in the first Brillouin zone. A connected Luttinger surface can be seen which lies partly on the AFZB (red dashed line) creating Luttinger arcs on the shifted Fermi surface. Here $\mu = 1.3$ and $\mathcal{V} = 1.5$

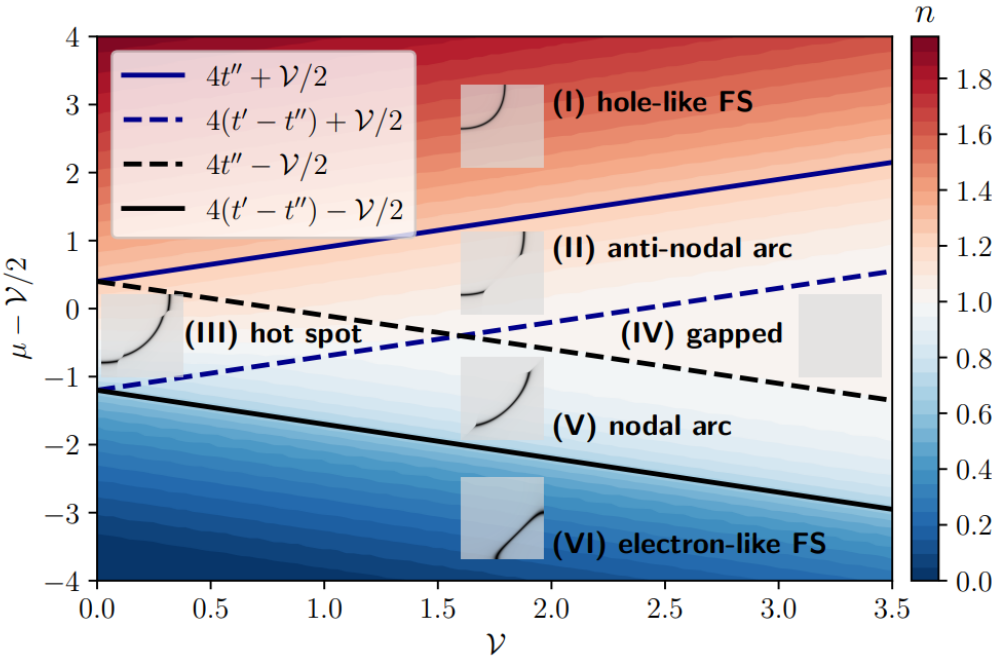

Figure 4.6: Phase diagram of the model Hamiltonian equation (4.1), different spectral functions are separated by dashed and solid lines given in terms of hopping parameters ($t = 1, t' = -0.2, t = 0.1$) and interaction potential $\mathcal{V}$. Different colors represent electron density. Taken from [18]

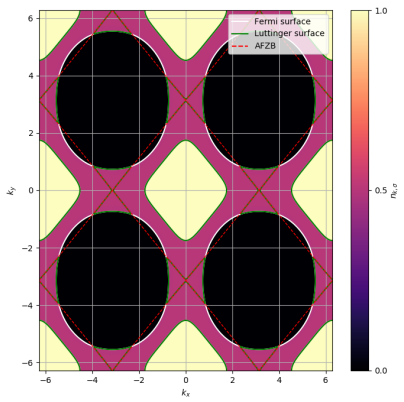

(a) Plot with color-bar for $\hat{n}_{\mathbf{k},\sigma}$

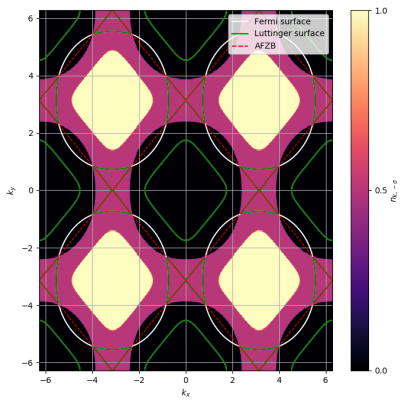

(b) Plot with color-bar for $\hat{n}_{\mathbf{k},-\sigma}$

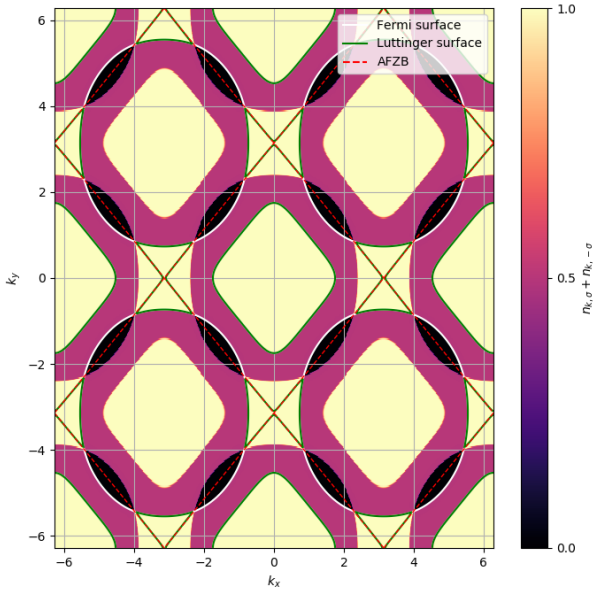

(c) Color-bar gives $\hat{n}_{\mathbf{k},\sigma} + \hat{n}_{\mathbf{k},-\sigma}$

Figure 4.7: Graphs showing occupation number in the ground-state, next to the Fermi and Luttinger surfaces in two brilouin zones. In white we see Fermi arcs in the nodal direction for $\mu = -0.3$ and $\mathcal{V} = 1.5$. We calculated average of number operator $\langle \hat{n}_{\mathbf{k},\sigma} \rangle$ as in equation 2.35 and plotted in k space (a). We see that in the $(T \to 0)$ limit we have only have three values for occupation: $\hat{n}_{\mathbf{k},\sigma} = 0$, $\hat{n}_{\mathbf{k},\sigma} = 1/2$ or $\hat{n}_{\mathbf{k},\sigma} = 1$ for zero, half and full occupation respectively. We also plot $\langle \hat{n}_{\mathbf{k},-\sigma} \rangle$ which is gives the same occupation in k but shifted in k with transfer momentum $Q = (\pi, \pi)$ (b). Adding them together gives the total occupation number in the ground-state (c). In the purple region for $\hat{n}_{k,\sigma} = \hat{n}_{k,-\sigma} = 1/2$ the spin is degenerate hence this region for double occupation (small yellow regions in $\hat{n}_{k,\sigma} + \hat{n}_{k,-\sigma}$ graph) it is not antiferromagnetic coupled, but spins align in a ferromagnetic way over transfer momentum $\mathbf{Q}$.

Chapter 5

Conclusion

In the first chapter we gave the initial motivation of the Hatsugai-Kohmoto model and it's properties. The non-local nature of the interaction in real space gives rise a local interaction in momentum space such that a Hamiltonian purely diagonal in momentum yields exact eigenstates. We saw how a two termed Green's function was exactly given by exact eigenstates of the Hamiltonian resulting in not only poles which corresponds to the spectral function, but also zero's. These zero's which arose by the cancellation of the two (non-interaction and interacting) terms in the single occupied region, also the Mott insulating phase. The Mott phase characterized by a degenerate ground-state due to spin degeneracy was is not an antiferromagnetic insulator phase as we have seen by performing spin correlation function. After considering the density of states of the HK model and retrieved the condition for half-filling, we gave the phase diagram for the given model. Here, different regions of occupation where separated by small increases of entropy in the metal phase.
In the first chapter we gave the initial motivation of the Hatsugai-Kohmoto model and it's properties. The non-local nature of the interaction in real space gives rise a local interaction in momentum space such that a Hamiltonian purely diagonal in momentum yields exact eigenstates. We saw how a two termed Green's function was exactly given by exact eigenstates of the Hamiltonian resulting in not only poles which corresponds to the spectral function, but also zero's. These zero's which arose by the cancellation of the two (non-interaction and interacting) terms in the single occupied region, also the Mott insulating phase. The Mott phase characterized by a degenerate ground-state due to spin degeneracy was is not an antiferromagnetic insulator phase as we have seen by performing spin correlation function. After considering the density of states of the HK model and retrieved the condition for half-filling, we gave the phase diagram for the given model. Here, different regions of occupation where separated by small increases of entropy in the metal phase.
In the first chapter we gave the initial motivation of the Hatsugai-Kohmoto model and it's properties. The non-local nature of the interaction in real space gives rise a local interaction in momentum space such that a Hamiltonian purely diagonal in momentum yields exact eigenstates. We saw how a two termed Green's function was exactly given by exact eigenstates of the Hamiltonian resulting in not only poles which corresponds to the spectral function, but also zero's. These zero's which arose by the cancellation of the two (non-interaction and interacting) terms in the single occupied region, also the Mott insulating phase. The Mott phase characterized by a degenerate ground-state due to spin degeneracy was is not an antiferromagnetic insulator phase as we have seen by performing spin correlation function. After considering the density of states of the HK model and retrieved the condition for half-filling, we gave the phase diagram for the given model. Here, different regions of occupation where separated by small increases of entropy in the metal phase.
In the first chapter we gave the initial motivation of the Hatsugai-Kohmoto model and it's properties. The non-local nature of the interaction in real space gives rise a local interaction in momentum space such that a Hamiltonian purely diagonal in momentum yields exact eigenstates. We saw how a two termed Green's function was exactly given by exact eigenstates of the Hamiltonian resulting in not only poles which corresponds to the spectral function, but also zero's. These zero's which arose by the cancellation of the two (non-interaction and interacting) terms in the single occupied region, also the Mott insulating phase. The Mott phase characterized by a degenerate ground-state due to spin degeneracy was is not an antiferromagnetic insulator phase as we have seen by performing spin correlation function. After considering the density of states of the HK model and retrieved the condition for half-filling, we gave the phase diagram for the given model. Here, different regions of occupation where separated by small increases of entropy in the metal phase.
In the first chapter we gave the initial motivation of the Hatsugai-Kohmoto model and it's properties. The non-local nature of the interaction in real space gives rise a local interaction in momentum space such that a Hamiltonian purely diagonal in momentum yields exact eigenstates. We saw how a two termed Green's function was exactly given by exact eigenstates of the Hamiltonian resulting in not only poles which corresponds to the spectral function, but also zero's. These zero's which arose by the cancellation of the two (non-interaction and interacting) terms in the single occupied region, also the Mott insulating phase. The Mott phase characterized by a degenerate ground-state due to spin degeneracy was is not an antiferromagnetic insulator phase as we have seen by performing calculations on the spin correlation function. After considering the density of states of the HK model and retrieving

the condition for half-filling, we gave the phase diagram for the given model. Here, different regions of occupation where separated by small increases of entropy in the metal phase.

The fact that the Green's function of the HK model has zero's and can potentially vanish at certain points hint on the fact that phenomena such as gaps in the Fermi surface may be explained by these zero's. This could actually be seen in the model discussed in chapter 3 where due to momentum dependent interaction in the HK model, changing Fermi surfaces in k space can cross such that a pseudogap appears. This has as a consequence that Luttinger's theorem is violated, because the Fermi surface is not closed.

In the last chapter a different model is considered which is based on the HK model. This model was able to capture the phenomenology of Fermi arcs as seen in APRES experiments in an exactly solvable model. Spin coupling of different momenta causes different eigenstates for the Hamiltonian, such that points k and $k+Q$ are either coupled to empty states or filled states depending on where we are in the Brillouin zone. Via the momentum coupled number operator $\hat{n}_{k+Q}$ Luttinger surfaces appear which are based on the notion of zero's explained in chapter 2. These zero's, now emerged as a result of coupling of different momenta separated by $Q = (\pi, \pi)$ will cover the Fermi surface on points in k space constrained by the relation $G_{k\sigma}(\omega = 0) = 0$. An antiferromagnetic zone boundary now disconnects the Fermi surface into a visible part and invisible Luttinger surface, where for a certain value of μ and $\mathcal{V}$ nodal Fermi arcs appear. That the Fermi arcs appear in the nodal direction, agrees with experimental findings as does the location of these cutoffs. Looking at the electron density on k we see that the surfaces consisting of Fermi and Luttinger arcs enclose the same areas in momentum space as was the case for the intact Fermi surface for the $Q = (0, 0)$ case (HK model). Although, these areas do not correspond to one particular ground-state in the Brillouin zone anymore. Eigenstates coupled through $k + Q$ result in a ground-state pattern in the Brillouin zone where the combined Luttinger+Fermi surfaces now enclose more than one ground-state energy. We see that the shape of the Fermi+Luttinger surface is exactly the same as for the HK model in contrast to the model we discussed in chapter 3.

Appendix A

Derivation of HK interaction in momentum space

First we write a discrete Fourier transform of the creation/annihilation operators

$$\hat{c}_{j\sigma} = \frac{1}{L^{d/2}} \sum_k e^{ik\cdot r_j} \hat{c}_{k\sigma}, \tag{A.1}$$

$$\hat{c}^\dagger_{j\sigma} = \frac{1}{L^{d/2}} \sum_k e^{-ik\cdot r_j} \hat{c}^\dagger_{k\sigma}. \tag{A.2}$$

The factor $L^{d/2}$ ensures that we still retrieve the usual commutation relation $[\hat{c}^\dagger_{j\sigma}, \hat{c}_{i\sigma}] = \delta_{j,i}$ and r_j is a position vector of the electron when going to momentum space. Substituting these in the Hamiltonian we get:

$$\hat{H}_{interaction} = \frac{\mathcal{V}}{L^d} \sum_{j_1,j_2,j_3,j_4} \delta_{j_1+j_3=j_2+j_4} \hat{c}^\dagger_{j_1\uparrow} \hat{c}_{j_2\uparrow} \hat{c}^\dagger_{j_3\downarrow} \hat{c}_{j_4\downarrow} \tag{A.3}$$

$$= \frac{\mathcal{V}}{L^d} \sum_{j_1..j_4} \delta_{j_1+j_3=j_2+j_4} \frac{1}{L^{2d}} \sum_{k_1..k_4} e^{-ik_1\cdot r_1} \hat{c}^\dagger_{k_1\uparrow} e^{ik_2\cdot r_2} \hat{c}_{k_2\uparrow} e^{-ik_3\cdot r_3} \hat{c}^\dagger_{k_3\downarrow} e^{ik_4\cdot r_4} \hat{c}_{k_4\downarrow} \tag{A.4}$$

$$= \frac{\mathcal{V}}{L^d} \sum_{j_1..j_4} \delta_{j_1+j_3=j_2+j_4} \frac{1}{L^{2d}} \sum_{k_1..k_4} e^{-i(k_1\cdot r_1 + k_3\cdot r_3)} e^{i(k_2\cdot r_2 + k_4\cdot r_4)} \hat{c}^\dagger_{k_1\uparrow} \hat{c}_{k_2\uparrow} \hat{c}^\dagger_{k_3\downarrow} \hat{c}_{k_4\downarrow} \tag{A.5}$$

$$= \frac{\mathcal{V}}{L^{3d}} \sum_{j_1..j_4} \delta_{j_1+j_3=j_2+j_4} \sum_{k_1..k_4} e^{-i(k_1+k_3)(r_1+r_3)/2} e^{-i(k_1-k_3)(r_1-r_3)/2} e^{i(k_2+k_4)(r_2+r_4)/2} e^{i(k_2-k_4)(r_2-r_4)/2} \hat{c}^\dagger_{k_1\uparrow} \hat{c}_{k_2\uparrow} \hat{c}^\dagger_{k_3\downarrow} \hat{c}_{k_4\downarrow} \tag{A.6}$$

Then a change the summation indices from $\sum_{j_1..j_4}$ to $\sum_{\alpha\beta\gamma\rho}$ where, $\alpha = r_1 + r_3$, $\beta = r_1 - r_3$, $\gamma = r_2 + r_4$ and $\rho = r_2 - r_4$ and a summation over sites $j_1..j_4$ is in principle a summation over the position vectors $r_1..r_4$. That way we get

$$\hat{H}_{interaction} = \frac{\mathcal{V}}{L^{3d}} \sum_{\alpha\beta\gamma\rho} \delta_{\alpha=\gamma} \sum_{k_1..k_4} e^{-i(k_1+k_3)\alpha/2} e^{-i(k_1-k_3)\beta/2} e^{i(k_2+k_4)\gamma/2} e^{i(k_2-k_4)\rho/2} \hat{c}^\dagger_{k_1\uparrow} \hat{c}_{k_2\uparrow} \hat{c}^\dagger_{k_3\downarrow} \hat{c}_{k_4\downarrow} \tag{A.7}$$

$$= \frac{\mathcal{V}}{L^{3d}} \sum_{\alpha\gamma} \delta_{\alpha=\gamma} \sum_{k_1..k_4} e^{-i(k_1+k_3)\alpha/2} L^d \delta_{k_1,k_3} e^{i(k_2+k_4)\gamma/2} L^d \delta_{k_2,k_4} \hat{c}^\dagger_{k_1\uparrow} \hat{c}_{k_2\uparrow} \hat{c}^\dagger_{k_3\downarrow} \hat{c}_{k_4\downarrow}, \tag{A.8}$$

Where in the second line we summed out $\beta = r_1 - r_3$ and $\rho = r_2 - r_4$ yielding the Dirac-delta terms and two times a factor L^d. Now we can sum out k_3 and k_4 to get

$$\hat{H}_{interaction} = \frac{\mathcal{V}}{L^d} \sum_{\alpha\gamma} \delta_{\alpha=\gamma} \sum_{k_1,k_2} e^{-i(k_1+k_1)\alpha/2} e^{i(k_2+k_2)\gamma/2} \hat{c}^\dagger_{k_1\uparrow} \hat{c}_{k_2\uparrow} \hat{c}^\dagger_{k_1\downarrow} \hat{c}_{k_2\downarrow}, \tag{A.9}$$

$$= \frac{\mathcal{V}}{L^d} \sum_{\alpha\gamma} \delta_{\alpha=\gamma} \sum_{k_1,k_2} e^{-ik_1\alpha} e^{ik_2\gamma} \hat{c}^\dagger_{k_1\uparrow} \hat{c}_{k_2\uparrow} \hat{c}^\dagger_{k_1\downarrow} \hat{c}_{k_2\downarrow}, \tag{A.10}$$

$$= \frac{\mathcal{V}}{L^d} \sum_{\alpha} L^d \sum_{k_1,k_2} e^{-i(k_1-k_2)\alpha} \hat{c}^\dagger_{k_1\uparrow} \hat{c}_{k_2\uparrow} \hat{c}^\dagger_{k_1\downarrow} \hat{c}_{k_2\downarrow}, \tag{A.11}$$

$$= \mathcal{V} \sum_{k_1,k_2} \delta_{k_1,k_2} \hat{c}^\dagger_{k_1\uparrow} \hat{c}_{k_2\uparrow} \hat{c}^\dagger_{k_1\downarrow} \hat{c}_{k_2\downarrow}, \tag{A.12}$$

$$= \mathcal{V} \sum_{k} \hat{c}^\dagger_{k\uparrow} \hat{c}_{k\uparrow} \hat{c}^\dagger_{k\downarrow} \hat{c}_{k\downarrow}. \tag{A.13}$$

Appendix B

Derivation of 2D dispersion with (next to- next) nearest neighbors

Equation 2.15 for nearest neighbor hopping is easily generalized to a 2D lattice considering hopping in the x and y direction

$$\hat{H}_{hopping} = -t \sum_{k} \sum_{\sigma} [e^{-ik_x} + e^{ik_x} + e^{-ik_y} + e^{ik_y}] \hat{c}^{\dagger}_{k\sigma} \hat{c}_{k\sigma} \tag{B.1}$$

$$= -2t \sum_{k,\sigma} \left(\cos(k_x) + \cos(k_y)\right) \hat{n}_{k\sigma}, \tag{B.2}$$

where $\epsilon_k = -2t\left(\cos(k_x) + \cos(k_y)\right)$. Next to nearest neighbors on a 2D lattice are located on the next point starting from site (i, j) and go in the diagonal direction. This means we go from sites (i, j) to

- $(i+1, j+1)$,
- $(i-1, j-1)$,
- $(i+1, j+1)$,
- $(i-1, j+1)$,

and we get the following contribution to the hopping Hamiltonian for including next to nearest neighbors

$$\hat{H}_{hopping} = -t' \sum_{k} \sum_{\sigma} \left[e^{i(k_x+k_y)} + e^{-i(k_x+k_y)} + e^{-i(k_x-k_y)} + e^{i(k_x-k_y)} \right] \hat{c}^{\dagger}_{k\sigma} \hat{c}_{k\sigma} \tag{B.3}$$

$$= -2t' \sum_{k\sigma} \left[\cos(k_x + k_y) \ + \cos(k_x - k_y)\right] \hat{n}_{k\sigma} \tag{B.4}$$

$$= -2t' \sum_{k\sigma} \left[2\cos(k_x)\cos(k_y)\right] \hat{n}_{k\sigma}. \tag{B.5}$$

For the next to next nearest hopping term we do the same as for the nearest term but we move two sites instead of one in the x and y direction. This only gives a factor of 2 extra

$$\hat{H}_{hopping} = -t'' \sum_{k\sigma} \left[e^{-2ik_x} + e^{2ik_x} + e^{-2ik_y} + e^{2ik_y} \right] \hat{c}^{\dagger}_{k\sigma} \hat{c}_{k\sigma} \tag{B.6}$$

$$= -t'' \sum_{k\sigma} 2(\cos(2k_x) + \cos(k_y)) \hat{n}_{k\sigma} \tag{B.7}$$

and will give a total hopping term of

$$\hat{H}_{hopping} = \sum_{k\sigma} \epsilon_k \hat{n}_{k\sigma} \tag{B.8}$$

with

$$\epsilon_k = -2t(\cos(k_x) + \cos(k_y)) - 4t' \cos(k_x)\cos(k_y) - 2t''(\cos(2k_x) + \cos(2k_y)), \tag{B.9}$$

Bibliography

[1] B. Batlogg, *The underdoped phase of cuprate superconductors.* `http://aiweb.techfak.uni-bielefeld.de/content/bworld-robot-control-software/`, 2000.

[2] J. G. Bednorz and K. A. Müller, *Possible high t_c superconductivity in the ba-la-cu-o system*, Zeitschrift für Physik B: Condensed Matter, 64 (1986), pp. 189–193.

[3] K. B. Dave, P. W. Phillips, and C. L. Kane, *Absence of luttinger's theorem due to zeros in the single-particle green function*, Physical Review Letters, 110 (2013).

[4] P. W. et. al., *Supplementary material for "Fermi and Luttinger arcs: two concepts, realized on one surface"*. https://synthical.com/article/Fermi-and-Luttinger-arcs [Online; accessed 10-02-2025].

[5] Y. Hatsugai and M. Kohmoto, *Exactly solvable model of correlated lattice electrons in any dimensions*, Journal of the Physical Society of Japan, 61 (1992), pp. 2056–2069.

[6] M. A. Hossain, J. D. F. Mottershead, A. Bostwick, J. L. McChesney, E. Rotenberg, R. Liang, W. N. Hardy, G. A. Sawatzky, I. S. Elfimov, D. A. Bonn, and A. Damascelli, *Controlling the self-doping of yba2c3o7-d polar surfaces: From fermi surface to nodal fermi arcs by arpes*, 2008.

[7] J. Hubbard, *Electron correlations in narrow energy bands*, Proceedings of the Royal Society of London, 276 (1963), p. 238.

[8] B. Keimer, S. A. Kivelson, M. R. Norman, S. Uchida, and J. Zaanen, *High temperature superconductivity in the cuprates*, 2014.

[9] J. M. Luttinger and J. C. Ward, *Ground-State Energy of a Many-Fermion System. II*, Physical Review, 118 (1960), pp. 1417–1427.

[10] D. S. Marshall, D. S. Dessau, A. G. Loeser, C.-H. Park, A. Y. Matsuura, J. N. Eckstein, I. Bozovic, P. Fournier, A. Kapitulnik, W. E. Spicer, and Z.-X. Shen, *Unconventional electronic structure evolution with hole doping in* $\mathrm{bi_2sr_2cacu_2}O_{8+\delta}$*: Angle-resolved photoemission results*, Phys. Rev. Lett., 76 (1996), pp. 4841–4844.

[11] N. F. Mott, *The basis of the electron theory of metals, with special reference to the transition metals*, Proceedings of the Physical Society, 62 (1949), p. 416.

[12] D. Nicoletti, O. Limaj, P. Calvani, G. Rohringer, A. Toschi, G. Sangiovanni, M. Capone, K. Held, S. Ono, Y. Ando, and S. Lupi, *High-temperature optical spectral weight and fermi-liquid renormalization in bi-based cuprate superconductors*, Phys. Rev. Lett., 105 (2010), p. 077002.

[13] M. R. Norman, H. Ding, M. Randeria, J. C. Campuzano, T. Yokoya, T. Takeuchi, T. Takahashi, T. Mochiku, K. Kadowaki, P. Guptasarma, and D. G. Hinks, *Destruction of the fermi surface in underdoped high-tc superconductors*, Nature, 392 (1998), p. 157–160.

[14] P. W. Phillips, L. Yeo, and E. W. Huang, *Exact theory for superconductivity in a doped mott insulator*, Nature Physics, 16 (2020), p. 1175–1180.

[15] S. Putilin, E. Antipov, and M. Marezio, *Superconductivity above 120 k in hgba2cacu2o6+*, Physica C: Superconductivity, 212 (1993), pp. 266–270.

[16] M. Shi, A. Bendounan, E. Razzoli, S. Rosenkranz, M. R. Norman, J. C. Campuzano, J. Chang, M. Månsson, Y. Sassa, T. Claesson, O. Tjernberg, L. Patthey, N. Momono, M. Oda, M. Ido, S. Guerrero, C. Mudry, and J. Mesot, *Spectroscopic evidence for preformed cooper pairs in the pseudogap phase of cuprates*, Europhysics Letters, 88 (2009), p. 27008.

[17] I. M. Vishik, *Photoemission perspective on pseudogap, superconducting fluctuations, and charge order in cuprates: a review of recent progress*, Reports on Progress in Physics, 81 (2018), p. 062501.

[18] P. Worm, M. Reitner, K. Held, and A. Toschi, *Fermi and luttinger arcs: Two concepts, realized on one surface*, Physical Review Letters, 133 (2024).

[19] K. Yang, *Exactly solvable model of fermi arcs and pseudogap*, Physical Review B, 103 (2021).